Journal of Molecular Graphics and Modelling 106 (2021) 107937

Contents lists available at ScienceDirect

Journal of Molecular Graphics and Modelling

journal homepage: www.elsevier.com/locate/jmgm

Discovery of novel isoform-selective histone deacetylases 5 and 9 inhibitors through combined ligand-based pharmacophore modeling, molecular mocking, and molecular dynamics simulations for cancer treatment

Ammar D. Elmezayen, Anas Al-Obaidi, Kemal Yelekçi *

Department of Bioinformatics and Genetics, Faculty of Engineering and Natural Sciences, Kadir Has University, 34083, Istanbul, Turkey

ARTICLE INFO

Keywords:
HDAC5
HDAC9
MD simulation
MM-PBSA
Pharmacophore modeling

ABSTRACT

Class IIa histone deacetylases (HDACs) 5 and 9 play crucial roles in several human disorders such as cancer, making them important targets for drug design. Continuous research is pursed to overcome the cytotoxicity side effect that comes with the currently available broad-spectrum HDACs inhibitors. Herein, common features of active HDACs inhibitors in clinical trials and use have been calculated to generate the best pharmacophore hypothesis. Guner-Henry scoring system was used to validate the generated hypotheses. Hypo1 of HDAC5 and Hypo2 of HDAC9 exhibited the most statistically significance hypotheses. Compounds with fit value of 3 and more were examined by QuickVina 2 docking tool to calculate their binding affinity toward all class IIa HDACs. A total of 6 potential selective compounds were subjected to 100 molecular dynamics (MD) simulation to examine their binding modes. The free binding energy calculations were computed according to the MM-PBSA method. Proposed selective compounds displayed good stability with their targets and thus they may offer potent leads for the designing of HDAC5 and HDAC9 isoform selective inhibitors.

1. Introduction

Epigenetics refers to the heritable changes in genetic materials that are not directly related to alterations in the DNA itself [1]. Such important changes include DNA methylation, histone post-transcriptional modifications, noncoding RNAs (ncRNAs) interactions and chromatin remodeling [2]. These crucial modifications significantly control the cell development in living organisms and aberrant regulation of these modifications can lead to several human disorders [3]. Histone proteins in eukaryotes, that play a vital role in DNA wrapping in the nucleus, are subjected do different modifications such as acetylation, phosphorylation and methylation [4]. Histone deacetylation is a well-studied mechanism in multicellular organisms and is regulated by a group of enzymes called histone deacetylases (HDAC), that act on the N-terminal of histone tails by removing the acetyl groups and results in more condensed chromatin [5]. HDAC enzymes are also known as lysine deacetylases (KDAC) due to their enzymatic activity in non-histone proteins [6]. Based on the sequence homology of HDACs to the yeast enzyme and domain organization, they are grouped into four subtypes. Classes I (HDACs 1, 2, 3, and 8) and II HDACs (class IIa 4, 5, 7, and 9; class IIb 6 and 10) are zinc-dependent enzymes that share sequence homology with the yeast reduced potassium dependency 3 (Rpd3) enzymes. HDAC11 is also a zinc-dependent enzyme yet does not share sequence homology with Rpd3 and thus is classified as class IV. Class III HDACs are called sirtuins and are nicotinamide adenine dinucleotide (NAD^+) [7–10].

Class IIa HDAC enzymes (HDACs 4, 5, 7, and 9) are exclusively expressed in particular cell types. HDAC4 expression is extremely seen in the epiphyseal plate and brain cells; HDAC5 and HDAC9 are highly expressed in the brain, heart, and muscle tissues; HDAC7 expression is highly notable in thymocytes and endothelial cells. Class IIa HDACs are characterized by a large noncatalytic N-terminal domain, which is responsible for assigning of class IIa HDACs to certain promoters and known for its regulatory role of the transportation of the enzymes between the cytoplasm and nucleus. This process is facilitated by the phosphorylation modification of the two conserved serine residues on the histone tail [11,12]. Genetic alterations to those conserved serine residues will lead to a nuclear delocalization of the class IIa HDACs and signal-refractory suppression of their target genes [13]. Class IIa HDACs are transported between the cytoplasm and nucleus during muscle

* Corresponding author. Kadir Has University, Faculty of Engineering and Natural Sciences, Bioinformatics and Genetics Departments, Cibali Campus, TR, 34083, Fatih, Istanbul, Turkiye.

E-mail addresses: amezyn81@gmail.com (A.D. Elmezayen), ib_ali2000@yahoo.com (A. Al-Obaidi), yelekci@khas.edu.tr (K. Yelekçi).

https://doi.org/10.1016/j.jmgm.2021.107937
Received 30 January 2021; Received in revised form 13 April 2021; Accepted 26 April 2021
Available online 20 May 2021

differentiation, which proves a precise role that each HDAC enzyme plays throughout the cell differentiation [14]. One of the characteristics of class IIa is the substitution of the tyrosine residue at the entrance to the lysine channel into histidine, as seen in HDAC4, 5, and 7, where this change affects the activity about a thousand degrees less compared to the rest of other HDACs. Unlike the side chain of tyrosine that is directed directly toward the active site and has an active role in the catalytic mechanism, the histidine side chain is directed away from the active site toward the solvent [15,16]. In addition to the catalytic zinc ion (Zn^{2+}) found in the active site of class I, II, and III HDACs, class IIa HDACs have a unique conserved structural zinc-binding subdomain. Remarkably, this zinc ion-binding subdomain has shown to play a critical role in the structural conformation of the catalytic domain of the protein. Two different conformations have been adopted by the zinc-binding subdomain: the inhibitor-free protein (apo-structure) namely "closed" conformation that might offer a path for the substrate to catalytic Zn^{2+} in the binding pocket; the inhibitor-bound protein namely "open" conformation [15,17,18].

Class IIa HDACs abnormal regulations have been associated with several human diseases such as cancer, immunological and neurological disorders, muscle degenerative and diabetes [19,20]. Hemizygously deletion in HDAC9 gene was involved in a minor ration of schizophrenia patients. HDAC9 has been reported to be profoundly expressed in mice brains exactly where the affected region by schizophrenia was observed [21]. HDAC5 was shown to be related to left ventricle hypertrophy and elevated salt intake. HDAC5 phosphorylation is induced by SIK1 activation upon elevated sodium concentrations, and consequently improves the transcriptional activity of MEF2 and nuclear factor of activated T-cells (NFAT) [22–24]. HDACs family has been well known for their association with the development of cancer. Vorinostat, one of the most famous pan-HDACs inhibitors, has been FDA-approved since 2006 for T-cell lymphoma treatment, signifying the importance of HDACs as targets for preventing cancer progression [25]. HDAC5 has been associated with tumor progression such as angiogenesis. In addition, survival of tumor tissues and cell proliferation in lung cancer were associated with the high expression rate of HDAC5 [26]. Another study reported an overexpression of HDAC5 in the estrogen receptor-positive (ER^{+}) tamoxifen-resistant MCF7-TamC3 breast cancer cell line [27]. Moreno and colleagues have demonstrated a correlation between the overexpression level of HDAC9 and the poor prognosis in childhood acute lymphoblastic leukemia (ALL) [28]. Several studies showed that the increased protein level of HDAC9 and its overexpression have been associated with different cancer cells including osteosarcoma, lymphoma, and breast cancer [29–31]. Additional investigation showed that altering survival and growth signaling pathways by manipulating the activity of p53 and B-cell lymphoma 6 (BCL6) might explain the HDAC9 contribution to lymphomagenesis [32].

With a closer look at the increasing number of scientific publications in recent years, HDACs have proven to be vital targets for anticancer drugs. The biological effect of inactivating HADCs in various types of cancers has shown their importance in treating cancer and reversing the pathological implications. HDAC known inhibitors are well established to control several molecular processes through regulating histone and non-histone proteins, including immune system response, cell cycle control, programmed cell death, and angiogenesis [33,34]. Nevertheless, their exact molecular mechanisms are still ambiguous [35]. The first pharmacophore model of HDAC inhibitors was established in 1997 by Jung et al. which led to the revolution of HDAC known inhibitors rational design. The mostly common and currently recognized HDAC known inhibitors pharmacophore features obey three main components: a zinc-binding group (ZBG) also known as chelator which can interact with catalytic zinc ion in the active site; a linker that normally mimics the acetyl-lysine and span through the substrate binding channel; and a cap group that is important for the isoform selectivity and also known as surface recognition domain (Fig. 1) [36–38].

However, the above pharmacophore model is not entirely applied for

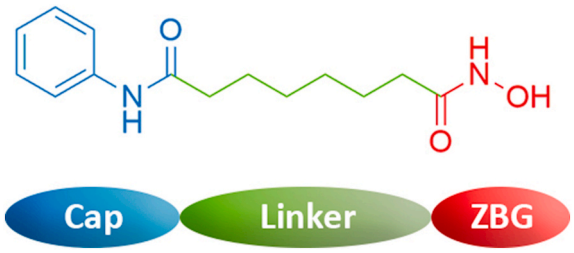

Fig. 1. HDACs inhibitors pharmacophore model features. The model represents the chemical structure of suberanilohydroxamic acid (SAHA), the HDAC inhibitor.

HDACs inhibitors that target other pockets besides the main active site such as lower pocket, foot pocket and side pocket. Hence, another pharmacophore model was proposed by Melesine et al., in 2018 which contains six components instead of three: surface cap S-cap, side pocket cap SP-cap, lower pocket LP-group, foot pocket FP-group, ZBG, and linker [39]. HDAC inhibitors can either display an isoform selectivity or can be pan inhibitors and non-selective. Generally, based on structural features, HDAC inhibitors are sub-grouped into benzamides, hydroxamic acids, cyclic peptides, and short chain fatty acids [36,40–43]. Four HDACs inhibitors are currently approved by the FDA. Vorinostat was the first HDACs inhibitor to be approved by FDA in 2006, which is a non-selective broad-spectrum HDAC inhibitor with IC_{50} of ~10 nM in cell-free assays and is used in treatment of patients with cutaneous T-cell lymphoma (CTCL) [44,45]. Romidepsin (FK228) was the second HDAC inhibitor to be approved by FDA in 2009, that shows a potent selectivity against HDACs 1 and 2 with IC_{50} of 36 nM and 47 nM in cell-free assays and is used in treating patients with CTCL and peripheral T cell lymphoma (PTCL) [46,47]. Belinostat (PXD101) was also approved in 2014 by FDA that is a broad-spectrum HDAC inhibitor with IC_{50} of 27 nM in a cell-free assay and is used in treating patients with PTCL [47,48]. Lastly, Panobinostat (LBH589) was approved by FDA in 2015, which shows an IC_{50} activity of 5 nM in a cell-free assay in HDACs and is used in treating patients with multiple myeloma [45,49]. Many class II HDACs inhibitors are currently in clinical trials for cancer treatment. Tasquinimod is a potent HDAC inhibitors which is prescribed for patients with castration-resistant prostate cancer (CRPC). Tasquinimod anticancer efficacy is assessed in phase III clinical trials [50–52]. MC1568 and MC1575 are aroyl-pyrrolyl–hydroxyamides (APHAs) derivative inhibitors. They were produced as a result of structural modifications in the linker group pf APHA [53–56]. MC1568 and MC1575 showed significantly lowered cytotoxic effect in comparison to classical class I HDAC inhibitors [55]. LMK235 is another class II HDACs inhibitors that was designed by a structural hybridization between the benzamides and the hydroxamic acids of class I HDAC inhibitors. The cap feature of LMK234, which consists of a dimethyl group, increased the selectivity of the drug toward HDACs 4 and 5 [57]. TMP195 and TMP269 are class IIa HDACs inhibitors that were obtained by replacing the classical hydroxamic acid group by a trifluoromethyloxadiazolyl group (TFMO), which improved the isoform selectivity toward class IIa HDAC enzymes [58]. Another example of class IIa inhibitors is BRD4354, which is a potent drug and consists of a hydroxyquinoline as the Zn^{2+}-triggered electrophile. BRD4354 shows half-maximal inhibitory concentration of 0.85 μM and 1.88 μM with HDAC5 and HDAC9, respectively [59]. BML-210 is moderate class IIa HDACs selective inhibitor that interacts with HDAC enzymes by its aminophenyl group [59]. Additional class IIa inhibitors include the 2-trifluoroacetylthiophenes derivative inhibitors, that were originally developed from ethyl 5-(trifluoroacetyl)thiophene-2-carboxylate to enhance the isoform selectivity toward class IIa enzymes [60]. CHDI-390576 is the newest reported class IIa HDAC inhibitor that displays half-maximal inhibitory concentration ranging between 0.031 and 0.051 μM. CHDI-390576 is a result of a structural modification in the cap region of the benzhydryl hydroxamic acids [61].

However, the above listed known inhibitors have shown cytotoxicity due to their pan activity. To overcome that dilemma, several efforts were made in order to design isoform selective inhibitors by applying various computational methods such as scaffold replacement approach [62], ligand- and structure-based virtual screening [63–65], pharmacophore modeling approach [66], flexible molecular docking, and 3D quantitative structure activity relationship (3D–QSAR) [43]. In the present research work, efforts were made to identify the common chemical features among HDACs known inhibitors in order to identify novel promising selective inhibitors by employing pharmacophore approach, virtual screening and molecular docking study, molecular dynamics (MD) simulation, and free binding energy calculation by MM-PBSA method (Fig. 2).

2. Materials and methods

Chemically, only certain portion of the drug is included in the interactions with proper target and is responsible for the biological activity. This portion is called "pharmacophore" [67]. Pharmacophore defines the chemical features of a drug that are vital for its biological effect [68].

2.1. Proteins setup and preparation

To date, there are no resolved 3D structures for HDAC5 or HDAC9. Thus, the 3D structures of human HDAC5 and HDAC9 from our previous homology modeling study [69] were used in the present research work. "Prepare Protein" wizard in BIOVIA Discovery Studio 4.5 (DS 4.5) [70] was utilized to prepare the proteins. The "Prepare Protein" protocol was applied to add missing atoms to incomplete amino acid residues, standardize atom labels, and to protonate titratable residues using predicted pKa using CHARMM force field.

2.2. Biological data: training set selection

For the pharmacophore modeling, two sets composed of 21 HDAC5 known inhibitors and 21 HDAC9 known inhibitors of diverse structures with a wide range of IC_{50} values ranging from 1 to 11,700 nM were collected from ChEMBL database (https://www.ebi.ac.uk/chembl/) [71] and several literatures [57,59,63,72–94]. These known inhibitors included: T009, Trichostatin, Cudc-101, LMK235, R306465, Dacinostat, Vorinostat, Tubastatin A, Chimera 4, Marbostat, ST2987, Entinostat, ST3049, Tubacin, Largazole, Azumamide E, Mocetinostat, HPB, redFK228, ST3710, Nexturastat A, BDBM119696, IYS-15, IYS-1, TMP269, IYS-14, BRD4354, BDBM218159, Fimepinostat, BDBM119709, Scriptaid, BDBM191641, BDBM124205, ST2741, and BDBM191640.2D structure of these known inhibitors are given in Supporting Information Figures SI1 and SI2. In addition, these known inhibitors involve a various structural components and are well studied against class IIa HDAC enzymes; thus, they were used to design the training data sets in order to create the pharmacophore models.

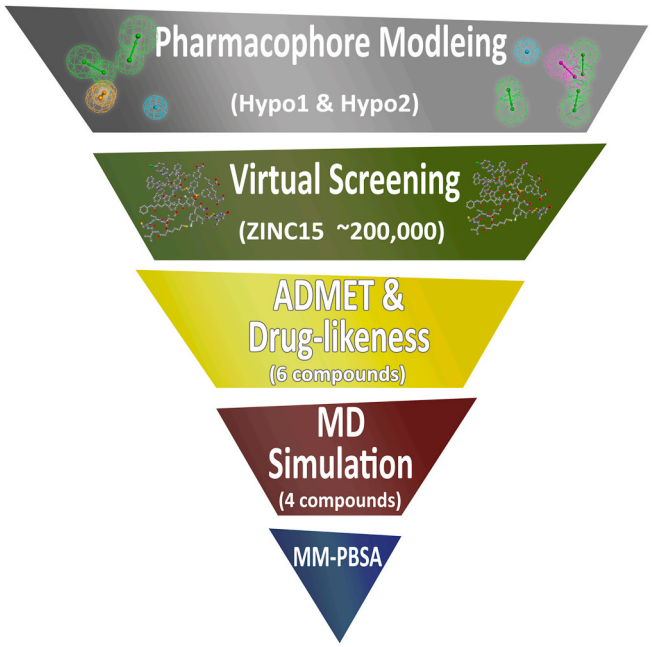

Fig. 2. Workflow scheme for pharmacophore modeling and virtual screening.

2.3. Pharmacophore hypothesis generation

The Catalyst tool provided by BIOVIA DS 4.5 was used to generate the ligand-based pharmacophore hypothesis in our research work, where HipHop algorithm was applied to generate the ten best pharmacophore hypotheses from the training set molecules. HipHop finds conformations and 3D spatial assemblies of chemical characteristics and features, which are shared by a set of chemical compounds [95]. Herein, previously reported HDACs known inhibitor LMK235 [57] was identified as a reference molecule for the training set used in the HDAC5-pharmacophore model generation. Similarly, BRD4354 compound [59] was set as a reference molecule the HDAC9-pharmacophore hypotheses generation. Both compounds were selected based on their inhibition activity toward HDACs 5 and 9, respectively. According to the successful pharmacophore hypothesis generated by Luo in 2016, the *principal* and *MaxOmitFeat* values for the reference molecules were set to 2 and 0, respectively. While the *principal* and *MaxOmitFeat* values for the rest of the training sets were put to 1 and 2, respectively [96]. The "BEST" module was applied in the conformational generation with energy threshold of 20 kcal/mol, where a maximum of 225 conformations was allowed for each molecule in the training sets. Each of the chemical features was given limits from a minimum of 1 to a maximum of 10 features. The minimum interfeature distance was set to 1 to guarantee the pharmacophore features proximity and the minimum feature point was set to 1. All other parameters were left at default values.

2.4. Validation of pharmacophore hypotheses by test sets

To assess the validity of the generated pharmacophore hypotheses, another 21 known HDAC5 inhibitors and 21 known HDAC9 inhibitors with a wide range of IC_{50} values ranging from 50 to 35,000 nM, which are not included in the training sets, were used in the test sets as active compounds [18,72–74,76,79,83–87,93,94,97–103]. The 2D structure of the compounds are included in Supporting Information Figures SI3 and SI4. The test sets consisted of diverse structures to assure the extent of pharmacophore reliability. The test sets used in current study included the FDA approved inhibitors such as Panobinostat and Romidepsin, inhibitors under different clinical trials such as Ricolinostat and CUDC-101, and other known inhibitors such as Largazole, Tubacin, TMP269, PBHA, Benzohydroxamate, and many others as shown in Supporting Information Figures SI3 and SI4. Technically, Catalyst HipHop tool in DS 4.5 defines common pharmacophoric features from training set compounds that are tested against the test set compounds. Fitting the test set compounds and mapping them onto the pharmacophore conformations is possible when their structural features and a minimum of one conformation can be matched within certain degrees of freedom of the related ideal spatial orientation. Generally, different forms of sets can be utilized to both generate and hypothetically validate the generated pharmacophore models. While known active compounds in the training set serve as a template for the generation of the pharmacophore model, other known active compounds are collected in the test set to investigate whether the build model will similarly map other active and inactive compounds besides those in the training set. Here comes the importance of the test set to validate the generated models.

Therefore, a pharmacophore model should also be able to filter-out inactive compounds beside its ability of identification of active compounds. For each of the molecules in the test sets, 10 decoys (inactive compounds) were generated using DecoyFinder program [104], which yielded a database of 231 compounds. Decoy sets were used to assess the best hypothesis and to decide whether the pharmacophore model can distinguish between potential HDACs inhibitors and other compounds. The decoy sets were used to validate the pharmacophore models by running each of the generated hypotheses against them and by calculating the goodness of hit (GH) using the following equations [105]:

$$Y\% = \frac{H_a}{H_t} \times 100\% \quad (1)$$

$$A\% = \frac{H_a}{A} \times 100\% \quad (2)$$

$$E = \frac{H_a \times D}{H_t \times A} \quad (3)$$

$$GH = \frac{H_a(3A + H_t)}{4H_t \times A} \times \left(1 - \frac{H_t - H_a}{A - D}\right) \quad (4)$$

Where $Y\%$ is the ratio of active compounds retrieved from the decoy set; H_a is the number of active compounds in the hit list; H_t is the total number of hit compounds in the decoy set; $A\%$ is the percentage of active compounds in the hits list; A is the total number of active compounds in the decoy set; E is the enrichment factor, D is the total number of compounds in the decoy set; and GH is the goodness of hit which determines the quality of generated hypotheses and is anticipated to yield a score between 0.6 and 1 for a reliable pharmacophore model [105].

2.5. Database screening for new hits

Database search was applied to identify candidate compounds that are likely to show activity against our targets. The best pharmacophore hypotheses were run against chemical database containing 200,000 molecules downloaded from ZINC15 website (http://zinc15.docking.org/) [106]. Based on the GH scores, HDAC5-pharmacophore Hypo1 and HDAC9-pharmacophore Hypo2 were run against the database using "BEST" search method provided by BIOVIA DS 4.5.

2.6. Molecular docking study

In order to evaluate the hit compounds obtained from the 3D database search and examine their interactions and binding poses within their respective targets, molecular docking method was conducted using QuickVina 2 [107]. QuickVina 2 is an enhanced molecular docking tool, which was developed from classic AutoDock Vina program [108]. According to the 3D database search results, HDAC5-pharmacophore Hypo1 retrieved 7966 hit compounds and HDAC9-pharmacophore Hypo2 retrieved 21,422 hit compounds, where these compounds showed fit values of 3.00 or more. Proteins and all small molecules were prepared and saved as PDBQT files using AutoDockTools [109]. AutoDockTools assisted in assigning Gasteiger charges and adding polar hydrogen atoms to both the proteins and the compounds. The size of the energy grid boxes for HDAC5 and HDAC9 was modified to include all active residues in the active site and was centered around the Zn^{2+} ion. XYZ coordinates and the energy grid boxes were set as follows: 19.199, −10.083, −1.089 and 22.5, 22.5, 22.5 Å, respectively.

2.7. ADMET profile, druglikeness, and PAINS filtration

ADMET profile was carried out for the lead compounds in order to evaluate the physiochemical properties using AdmetSAR server (http://lmmd.ecust.edu.cn/admetsar2) such as logP, water solubility and Caco-2 cell membrane permeability [110]. SwissADME server (http://www.swissadme.ch/) was utilized to predict the druglikeness according to Lipinski's "Rule of 5", which is essential in computational drug design [111,112]. SMILES format of the candidates was used as input files for the ADMET profile prediction. The advances in high-throughput screening in computer-aided drug design have accelerated the drug discovery process and the identification of new compounds as active leads, however, many of these leads are eliminated due to their false positive impacts. These leads may contain certain sub-structures that were demonstrated by Baell and Holloway as pan assay interference compounds (PAINS) [113]. These substructure features have the ability to interact and bind to random targets with unspecific manner which results in false positives. To guarantee that the studied hit compounds are free of PAINS, the PAINS Remover website (https://www.cbligand.org/PAINS/) was used in the present study [113].

2.8. Molecular dynamic (MD) simulation

The free forms of HDAC5 and HDAC9 along with their respective protein-ligand complexes were subjected to MD simulations using Nanoscale Molecular Dynamics software 2.13 (NAMD) [114] in order to analyze the complex stability and evaluate the structural changes. The best binding poses of all four protein-ligand complexes from Vina were used to generate the input files for the MD simulation using Chemistry at Harvard Macromolecular Mechanics web-based graphical user interface (CHARMM-GUI) (http://www.charmm-gui.org/) [115–117]. The force field CHARMM36 m was applied to all simulations in this study [118], and the CHARMM General Force Filed (CGenFF) was utilized to generate and prepare parameter files for the leads (https://cgenff.umaryland.edu/) [119–122]. All systems were solvated by Transferable Intermolecular Potential 3 (TIP3) water molecules and neutralized by NaCl ions. For each system, the energy was minimized by steepest descent method for 10,000 steps and equilibrated under constant number of atoms, volume, and temperature (NVT) ensemble for 10 ns with reference temperature of 310 K. Finally, unrestrained 100 ns MD simulations were performed under constant number of atoms, pressure, and temperature (NPT) ensemble for all systems with reference temperature of 310 K. All MD trajectories were analyzed using Visual Molecular Dynamics software (VMD) [123].

2.9. Free binding energies calculation

In order to calculate the binding free energy of protein-ligand complexes, molecular mechanics Poisson-Boltzmann Surface Area (MM-PBSA) method was conducted using Calculation of Free Energy (CaFE) tool [124]. CaFE tool is easy-to-use tool and efficient in running different MD trajectory file types and can support numerous force field parameters [125–127]. The binding free energy (ΔG_{bind}) involves three energetic factors: gas-phase free energy (ΔG_{MM}), solvation free energy (ΔG_{sol}) and the change in the system entropy ($-T\Delta S$) and can be calculated according to the following equations [128]:

$$\Delta G_{bind} = \Delta G_{MM} + \Delta G_{sol} - T\Delta S \quad (5)$$

$$\Delta G_{bind} = \Delta E_{vdw} + \Delta E_{elec} + \Delta G_{polar} + \Delta G_{nonpolarc} - T\Delta S \quad (6)$$

For each system, the energy elements were calculated using 200 snapshots extracted from the last 10 ns of MD trajectory files. The internal dielectric constant was set to 4, the external dielectric constant was 80 and the reciprocal of grid spacing was 1 Å. All other parameters were used as default.

3. Results and discussion

3.1. Generated pharmacophore hypotheses

One of the important methods in modern computer-aided drug

design is the pharmacophore modeling, which has become a vital tool for in silico drug discovery. The HipHop method has been widely used in pharmacophore modeling and effectively applied in exploring novel inhibitors against several biological systems [129–131]. The 10 generated pharmacophore models based on HDAD5 known inhibitors consist of the same five features: 1 hydrophobic (aromatic/aliphatic); 1 hydrogen bond donor; and 3 hydrogen bond acceptor groups (Supporting Information Figure SI5). Among the generated hypotheses, Hypo1 showed the top rank value (Table 1) and displayed the highest GH score (0.86) and enrichment factor (10.26) (Table 2). The five pharmacophore features of Hypo1 were found to be well mapped onto the following HDAC5 known inhibitors that were included in the training set: LMK235, Chimera 4, HPB, R306465, Cudc-101, Dacinostat, Vorinostat, T009, Trichostatin A, Marbostat, Tubastatin A, ST3049, Tubacin, ST3710, Azumamide E, ST2987, redFK228, Largazole, and Nexturastat A. Consequently, Hypo1 of HDAC5 displayed the most statistically significance hypothesis where it yielded 93% of the active compounds. The 3D database search against the Hypo1 retrieved a total of 7996 compounds, that showed fit value of 3 or more and met the geometric constrictions of Hypo1 and well mapped onto the hypothesis with their unique scaffolds.

The other 10 generated pharmacophore hypotheses based on HDAD9 known inhibitors consist of several features: ring aromatic, hydrophobic (aromatic/aliphatic), hydrogen bond donor; and hydrogen bond acceptor groups. Although Hypo2 is statistically ranked as the second (Table 3), it exhibited the highest GH score (0.87) and enrichment factor (10.13) (Table 4). The four generated pharmacophore features of Hypo2 include: 1 ring aromatic; 1 hydrophobic (aromatic/aliphatic); and 2 hydrogen bond acceptor groups. HDAC9 known inhibitors form the training set were found to be well mapped onto Hypo2 including BRD4354, BDBM191640, BDBM191641, TMP269, Fimepinostat, ST2741, BDBM119709, R306465, BDBM119696, Scriptaid, Tubastatin A, IYS-14, BDBM124205, ST2987, BDBM218159, IYS-1, T009, Dacinostat, IYS-15, and Vorinostat (Supporting Information)Figure SI6. Hypo2 of HDAC9 was found to be the most statistically significance hypothesis as it yielded 93% of the active compounds. A total of 21,422 compounds were retrieved from the 3D database search and showed 3 or more fit value and fitted the geometric constrictions of Hypo2 and well represented onto the hypothesis with their characteristic scaffolds.

3.2. Molecular docking study

Hypo1 of HDAC5 and Hypo2 of HDAC9 were screened against a total of ~200,000 drug-like diverse structure compounds from ZINC15 database. The 3D database search retrieved ~7000 compounds for Hypo1 and ~21,000 for Hypo2, all with fit value of 3 and above, which was calculated and ranked by the Catalyst tool in BIOVIA DS 4.5. The yielded compounds were further examined by the molecular docking approach in an attempt to predict their best binding modes. The molecular docking analysis revealed a total of 3 top-ranked isoform selective compounds for each of HDACs 5 and 9 (Table 5). All six compounds were well mapped onto their respective pharmacophore

Table 1
Common features of the 10 generated pharmacophore hypotheses for the HDAC5 known inhibitors.

Hypotheses	Features	Rank	Max. Fit
1	HDAAA	256.83	5
2	HDAAA	246.53	5
3	HDAAA	246.00	5
4	HDAAA	245.70	5
5	HDAAA	244.02	5
6	HDAAA	243.54	5
7	HDAAA	242.87	5
8	HDAAA	242.79	5
9	HDAAA	241.73	5
10	HDAAA	241.09	5

H: hydrophobic (aromatic/aliphatic); D: hydrogen bond donor; A: hydrogen bond acceptor.

Table 2
Guner-Henry scoring method results for validating the 10 generated pharmacophore hypotheses based on the HDAC5 known inhibitors.

Hypotheses	D [a]	A [b]	H_t [c]	H_a [d]	A% [e]	Y% [f]	E [g]	GH [h]
1	231	21	15	14	66.66	93.33	10.26	0.862
2	231	21	16	13	61.90	81.25	8.93	0.753
3	231	21	18	14	66.66	77.77	8.55	0.735
4	231	21	18	14	66.66	77.77	8.55	0.735
5	231	21	15	13	61.90	86.66	9.53	0.797
6	231	21	21	14	66.66	66.66	7.33	0.644
7	231	21	15	13	61.90	86.66	9.53	0.797
8	231	21	18	14	66.66	77.77	8.55	0.735
9	231	21	17	14	66.66	82.35	9.05	0.773
10	231	21	19	13	61.90	68.42	7.52	0.648

[a] D: the sum of the compounds presents in the decoy set.
[b] A: the sum of the active compounds in the decoy set.
[c] Ht: the total number of the hits within the decoy set.
[d] Ha: the total number of the active compounds shown in the hit list.
[e] A%: the ratio of the active compounds within the hits list.
[f] Y%: the ratio of the active compounds identified by the pharmacophore model from the decoy set.
[g] E: the enrichment factor.
[h] GH: the goodness of hit.

Table 3
Common features of the 10 generated pharmacophore hypotheses for the HDAC9 known inhibitors.

Hypotheses	Features	Rank	Max. Fit
1	RHAA	176.23	4
2	RHAA	173.68	4
3	RHAA	169.77	4
4	RHAA	169.26	4
5	RHAA	167.30	4
6	HHDA	166.70	4
7	RHAA	164.71	4
8	RHAA	163.55	4
9	HHAA	162.50	4
10	RHAA	162.43	4

R: aromatic ring; H: hydrophobic (aromatic/aliphatic); D: hydrogen bond donor; A: hydrogen bond acceptor.

Table 4
Guner-Henry scoring method results for validating the 10 generated pharmacophore hypotheses based on the HDAC9 known inhibitors.

Hypotheses	D [a]	A [b]	H_t [c]	H_a [d]	A% [e]	Y% [f]	E [g]	GH [h]
1	231	21	18	15	71.42	83.33	9.166	0.792
2	231	21	16	15	71.42	93.75	10.31	0.877
3	231	21	18	16	76.19	88.88	9.777	0.848
4	231	21	19	15	71.42	78.94	8.684	0.755
5	231	21	19	15	71.42	78.94	8.684	0.755
6	231	21	35	18	85.71	51.42	5.657	0.551
7	231	21	37	19	90.47	51.35	5.648	0.558
8	231	21	20	15	71.42	75.00	8.250	0.723
9	231	21	32	17	80.95	53.12	5.843	0.557
10	231	21	16	14	66.66	87.50	9.625	0.815

[a] D: the sum of the compounds presents in the decoy set.
[b] A: the sum of the active compounds in the decoy set.
[c] Ht: the total number of the hits within the decoy set.
[d] Ha: the total number of the active compounds shown in the hit list.
[e] A%: the ratio of the active compounds within the hits list.
[f] Y%: the ratio of the active compounds identified by the pharmacophore model from the decoy set.
[g] E: the enrichment factor.
[h] GH: the goodness of hit.

Table 5
Reference compounds (LMK235, BRD4354) and the top-ranked compounds with their calculated binding energy using QuickVina 2. Selective isoform compounds for HDACs 5 and 9 are presented in bold.

#	Compound ID	HDAC4	HDAC5	HDAC7	HDAC9
		ΔG (kcal/mol)	ΔG (kcal/mol)	ΔG (kcal/mol)	ΔG (kcal/mol)
Comp1	ZINC000257282664	−7.4	**−8.9**	−7.8	−7.7
Comp2	ZINC000008918470	−7.6	**−8.9**	−7.6	−7.6
Comp3	ZINC000035354144	−7.1	**−8.1**	−6.5	−7
Comp4	ZINC000016012342	−9.2	−8.7	−8.8	**−10.3**
Comp5	ZINC000020942817	−8.1	−8.1	−7.3	**−9.3**
Comp6	ZINC000001264757	−6.8	−7	−6.7	**−8**
7	LMK235	–	−6.8	–	-
8	BRD4354	–	–	–	−7.3

hypothesis and their fit values are shown in Fig. 3. The 2D structures of the four selected top-ranked compounds are illustrated in Fig. 4. Hypo1 and Hypo2 agreed with the classical pharmacophore features of HDAC inhibitors [40]. The cap/linker/chelator characteristic of classic HDAC inhibitors was well exemplified by Hypo1 and Hypo2. Hydrophobic feature was found to be mapped onto the cap group; hydrogen bond acceptor mapped onto the linker of Hypo1, while aromatic ring onto the linker of Hypo2; hydrogen bond donor and acceptor feature mapped onto the chelator group. These findings agreed with the common pharmacophoric features of HDAC inhibitors [132].

The top two HDAC5 selective compounds, Comp1 and Comp2 (Fig. 4 (a)) exhibited the higher binding affinity toward HDAC5 and lowest binding energy with a score of −8.9 kcal/mol and a predicted inhibitory constant (K_i) of 294 nM for both compounds (Table 5). Both compounds proved to have lower binding energies toward HDAC5 compared to the reference known inhibitor used in this study, the LMK235, which showed a binding energy of −6.8 kcal/mol. Even though these two compounds are not structurally similar to most HDACs known inhibitors with their distinctive zinc binding groups, they both well spanned in the active site of HDAC5. Comp1 was found to be bonded to the active site via several key interactions including five hydrogen bonds with Arg155, His159, Phe169, Gly331 and Gly332; a π-sulfur interaction with Cys170; a π-π stacked interaction with Phe169; two π-alkyl interactions with Pro156 and Pro157 in addition to many van der Waals interactions

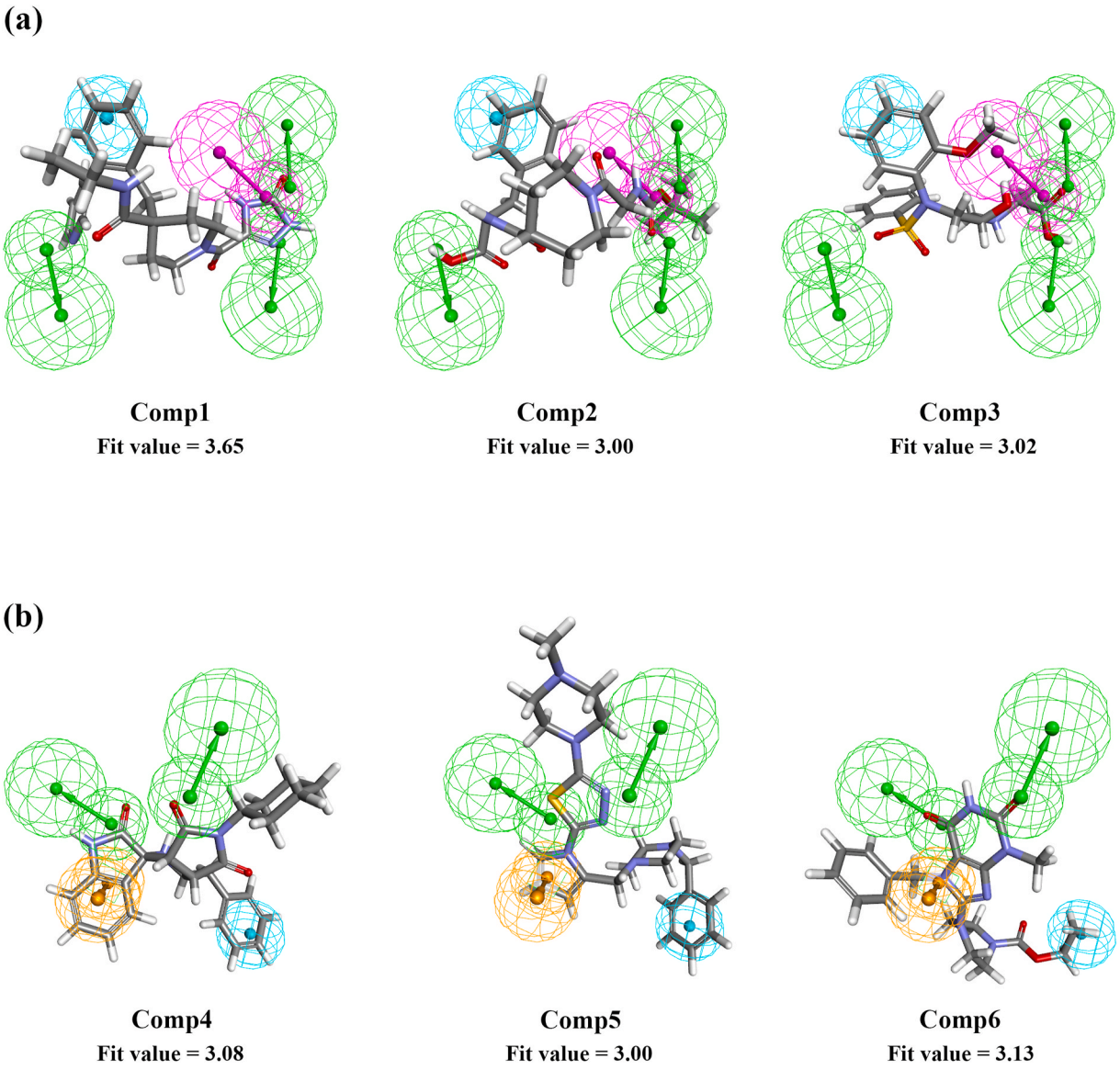

Fig. 3. The top six selective inhibitors and their mapping onto their respective pharmacophore hypothesis. (a) HDAC5 selective inhibitors mapped onto Hypo1. (b) HDAC9 selective inhibitors mapped onto Hypo2. **[2-column fitting image]**.

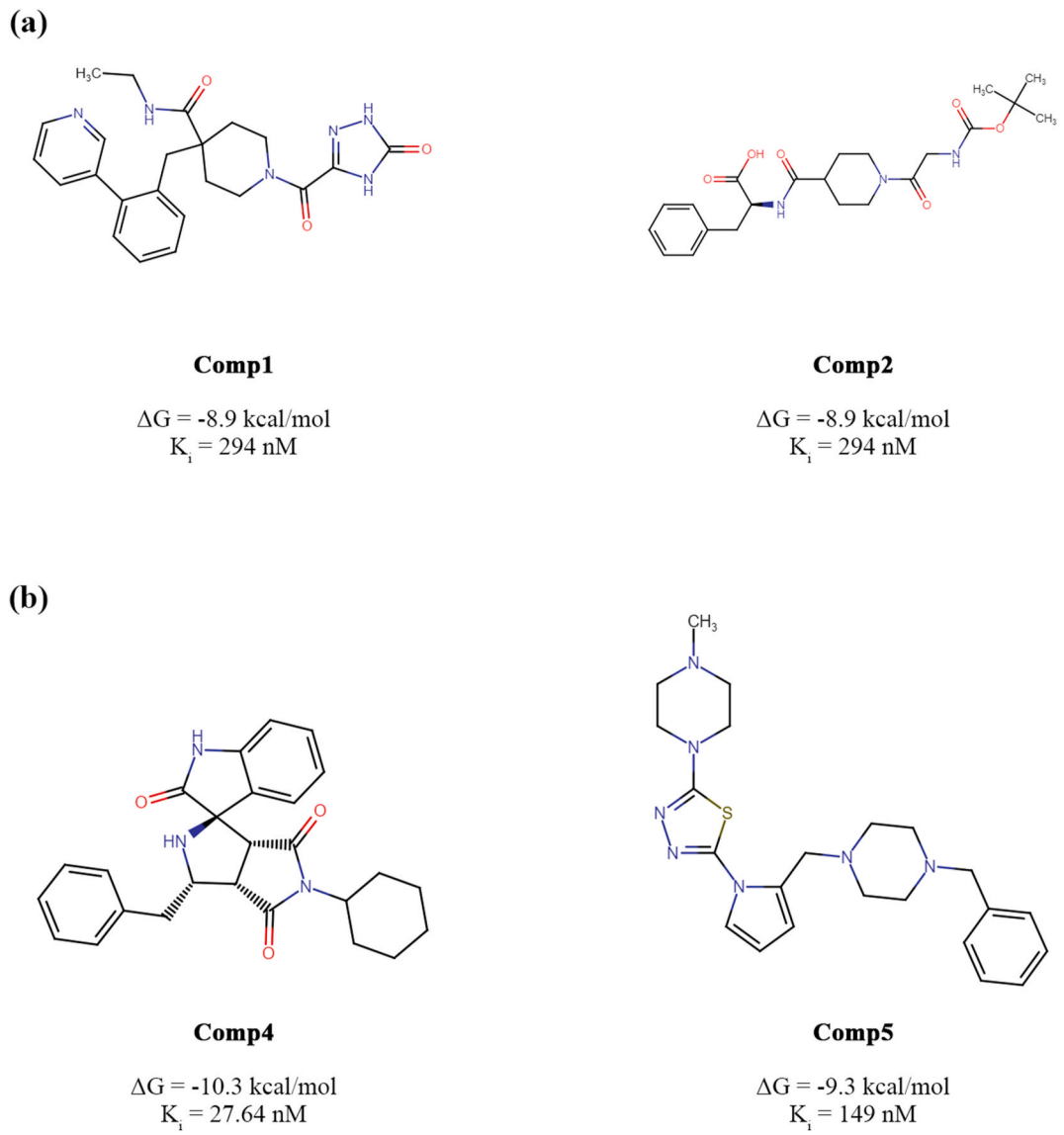

Fig. 4. 2D presentations of the selected top-ranked compounds: (a) HDAC5 selective inhibitor, (b) HDAC9 selective inhibitors.

(Fig. 5 (a)). Similarly, binding mode analysis of Comp2 revealed several important chemical interactions with HDAC5 including seven hydrogen bonds with Arg37, Arg155, Pro157, His159, His160, Asp291 and Gly331; a π-π stacked interaction with Phe228; two π-alkyl interactions with Phe169; an alkyl interaction with Pro156 and other several van der Waals interactions (Fig. 5 (b)). The catalytic zinc atom was observed to be bonded to both compounds via van der Waals interaction.

The molecular docking study showed Comp4 and Comp5 (Fig. 4 (b)) with the highest binding affinities toward HDAC9 and with the lowest binding energies of −10.3 kcal/mol and −9.3 kcal/mol, respectively (Table 5). The predicted inhibitory constants (K_i) of Comp4 and Comp5 were found to be of 27.64 nM and 149 nM, respectively. Interestingly, both top-ranked compounds displayed lower binding energies in comparison to the reference known inhibitor, BRD4354, which displayed a binding energy of −7.3 kcal/mol. Comp4 binding mode was found to be well fitted into the catalytic pocket of HDAC9 with the following significant interactions: one hydrogen bond with Arg155, π-π stacked interaction with Phe169 and one π-π T-shaped interaction with Phe169 as well, and many other van der Waals interactions. The catalytic zinc metal atom was not seen involved in any chemical interactions with the Comp4 (Fig. 5 (c)). Comp5 was perfectly spanned into the HDAC9 active site and showed several prominent interactions with the key amino acid residues including hydrogen bonds with Arg37 and Asp291; π-cation interaction with Arg39; π-alkyl interaction with Pro157, Phe169 and His199; π-π T-shaped interaction with His199; π-π stacked interaction with Phe228; van der Waals interaction with the catalytic zinc atom as well as many other amino acid residues (Fig. 5 (d)).

3.3. Selection criteria of the isoform-selective compounds

In 2008, Bieliauskas and Pflum demonstrated the selectivity index of many different HDACs known inhibitors in their study by comparing the inhibition constant of a particular HDAC protein to other HDAC members [133]. Thus, the selection process of the HDAC-selective inhibitors in the present study was inspired by Bieliauskas and Pflum research work. This was achieved by comparing the value of the inhibition constant of a particular inhibitor for a selected HDAC enzyme to other inhibition constants of the same inhibitor for other HDAC members. The following formula was applied to obtain the selectivity index, where "x" refers to the selected compound:

$$Selectivity\ of\ "x"\ for\ HDAC5\ or\ 9 = \frac{K_i\ of\ other\ HDACs\ isoform}{K_i\ of\ HDAC5\ or\ 9} \quad (7)$$

The selectivity index of HDAC5 and HDAC9 are given in Table 6.

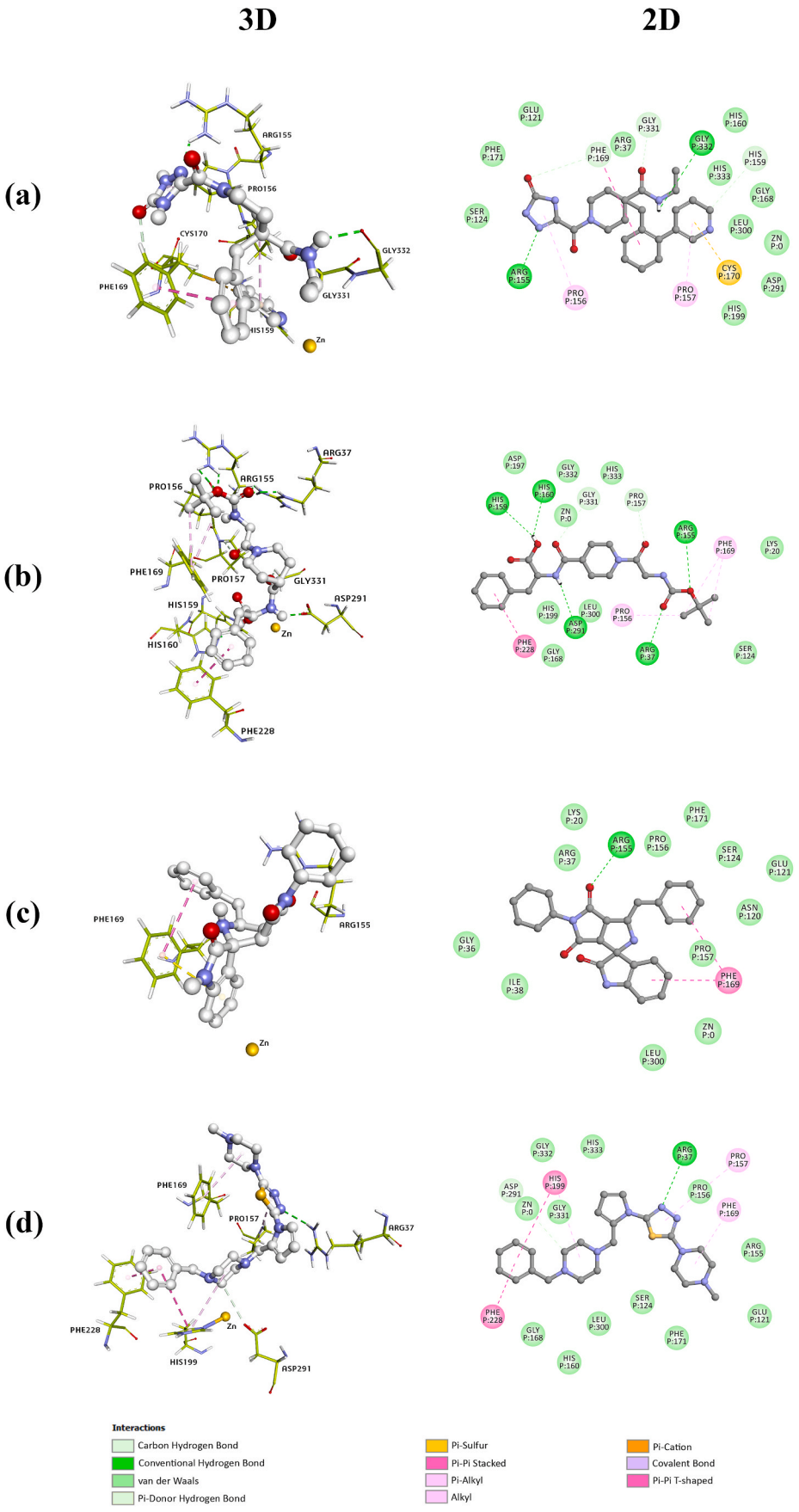

Fig. 5. 3D and 2D presentation of the chemical interactions of (a) Comp1, (b) Comp2, (c) Comp4, and (d) Comp5.

Table 6
Selectivity index of class IIa HDACs 5 and 9. Inhibition constant of one HDAC is compared to the closest inhibition constant of other HDACs for the same inhibitor.

	HDAC4	HDAC5	HDAC7	HDAC9	Selectivity
Compounds	K_i^4(nM)	K_i^5(nM)	K_i^7(nM)	K_i^9(nM)	
Comp1	3713	294	1888	2236	HDAC5
Comp2	2648	294	2648	2648	HDAC5
Comp3	6164	1137	16989	7299	HDAC5
Comp4	177	412	348	27.64	HDAC9
Comp5	1137	1137	4396	149	HDAC9
Comp6	10233	7299	12117	1347	HDAC9

Comp1 showed a potential selectivity toward HDAC5 ranging between ~7 and 13-fold compared to other members of class IIa HDACs. Comp2 displayed a ~9-fold isoform selectivity for HDAC5 over all members of class IIa. Comp4 revealed promising selectivity for HDAC9 ranging between ~7 and 15-fold over the other class IIa HDAC members. Lastly, Comp5 displayed a ~8 to 30-fold isoform selectivity for HDAC9 compared to the rest of the class IIa HDACs.

3.4. Drug-likeness prediction and PAINS filtration

Table 7 shows the physiochemical and drug-likeness properties of the isoform selective compounds. All the six selected compounds were found to be within the acceptable reference of oral drugs and thus can be classified as drug-like compounds. These compounds obeyed the famous Lipinski's rule of five, which states that oral drugs must have a molecular wight (MW) of 500 Da or less, the octanol-water partition coefficient (LogP) should not be more than 5, the total number of hydrogen bond donors should not be more than 5, and the total number of hydrogen acceptors must not be more than 10. Violating two or more of the previous criteria mostly result in poor permeable drugs [134]. According to the collected properties of 90% of 1700 oral drugs, Di and Kerns proposed the following criteria for identifying drug-like compounds: the water/aqueous solubility (LogS) should be larger than −5.7, the permeability rate in Caco-2 cell line must be faster than 22 nm/s, and lastly, the total number of the primary metabolites must not exceed 7 [135]. The topological polar surface area (TPSA) should not be more than 140 $Å^2$. Aqueous solubility of a drug compound, which is one of the ADMET descriptors, has a great impact on the transportation and the absorption of a drug compound in the biological systems. Quantitative structure–property relationships (QSPR) is effectively utilized to associate organic- and drug compounds to their corresponding water solubility [136]. Another ADMET property is the Caco-2 permeability, that describes the gastrointestinal permeability ration by predicting the degree of a drug compound transportation across the Caco-2 cell line [136]. Caco-2 permeability level has been predicted in a variety of drug compounds and drug-like molecules in silico and in vitro [137–140]. Moreover, the selected six compounds were found to be PAINS free compounds.

3.5. Analysis of the MD simulations

The structural stability of the docked complexes of HDAC5 with Comp1 and Comp2, HDAC9 with Comp4 and Comp5 were analyzed by evaluating their RMSD, RMSF, Rg, potential energy, and by assessing the number of the hydrogen bonds throughout the MD simulations.

3.5.1. RMSD analysis

The root mean squared deviation plots of the apo-protein of the HDAC5 and its complex systems with the known inhibitor (LMK235), Comp1, and Comp2 are shown in Fig. 6 (a). All the studied systems exhibited steady equilibrium state throughout the MD simulations. The RMSD of the apo-protein of HDAC5 (without inhibitor) slightly increased to 3.4 Å around the first 12 ns of the MD run then remained in equilibrium state until the end with an average RMSD of 3.2 Å. The RMSD of HDAC5 complexed with the known inhibitor rose from 0 Å to ~4.8 Å until 39 ns and then the RMSD decreased to an average of 4.1 Å and remained stable to the end. The backbone of the HDAC5-Comp1 complex showed an increased RMSD profile compared to the apo-protein where the system stabilized with an average RMSD of 4.7 Å after the first 44 ns of the simulation. Interestingly, the backbone RMSD of the HDAC5-Comp2 complex displayed similar trend with the apo-protein after the first 22 ns and remained stable until the end of the run. HDAC5-Comp2 complex showed lower RMSD profile over time of the MD run compared to HDAC5-Comp1 complex.

The RMSD profiles of the free HDAC9 protein and its complex systems with the BRD4354, Comp4 and Comp5 are shown in Fig. 6 (b). The backbone RMSD of the HDAC9 apo-protein initially increased to 5.2 Å around 37 ns and the system seemed to be stabilized until the end of the run with an average RMSD of 4.1 Å. The RMSD examination of Comp4 and Comp5 revealed that both systems showed comparable fluctuation after the first 50 ns and restrained their equilibrium state until the end of the MD simulation. HDAC9-Comp5 complex system gained its stability at earlier stages (around 16 ns) compared to HDAC9-Comp4 and had an average backbone RMSD of 3.9 Å. HDAC9-Comp4 complex system showed a slightly higher fluctuation until the 68 ns, but thereafter showed better equilibrium state until the end of the 100 ns run.

3.5.2. RMSF analysis

The root mean squared fluctuation (RMSF) analysis was conducted for the HDAC5 and HDAC9 complex systems and the results are presented in Fig. 7 (a) and (b), respectively. RMSF analysis helps in examining the local movements of amino acid residues and their behavior through the MD simulation. Higher backbone RMSF fluctuations were seen in loop regions that are known for their high flexibility. Overall, HDAC5-Comp2 complex system exhibited lower RMSF profile compared to the HDAC5-Comp1 complex system throughout the

Table 7
The druglikeness and the physiochemical properties of the 6 isoform selective compounds.

Compound	PAINS	MW [a]	HA [b]	HD [c]	LogP	TPSA [d]	HIA [e]	Caco-2	AQ [f]
Comp1	0	434.4	5	3	1.49	123.84	0.953	0.837	−3.059
Comp2	0	433.5	6	3	0.93	125.04	0.860	0.849	−3.146
Comp3	0	408.4	7	3	−1.35	124.55	0.945	0.535	−3.555
Comp4	0	429.5	4	2	3.03	78.51	0.972	0.779	−3.911
Comp5	0	437.6	5	0	2.22	71.91	0.989	0.571	−3.013
Comp6	0	412.4	5	1	1.44	105.46	0.969	0.647	−3.717

[a] MW: Molecular weight, Da.
[b] HA: Total number of H-bond acceptors, O and N.
[c] HD: Total number of H-bond donors, OH and NH.
[d] TPSA: Topological polar surface area, $Å^2$.
[e] HIA: Human intestinal absorption.
[f] AQ.: Water solubility, LogS.

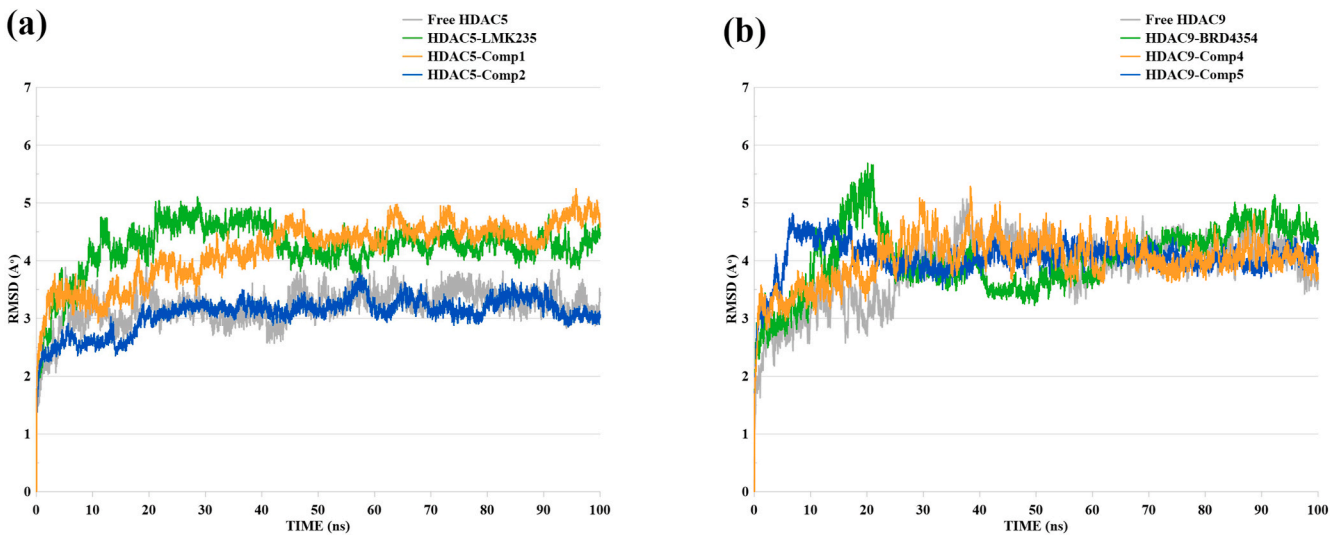

Fig. 6. Presentation of the root mean squared deviation (RMSD) for (a) HDAC5 complex systems; and (b) HDAC9 complex systems..

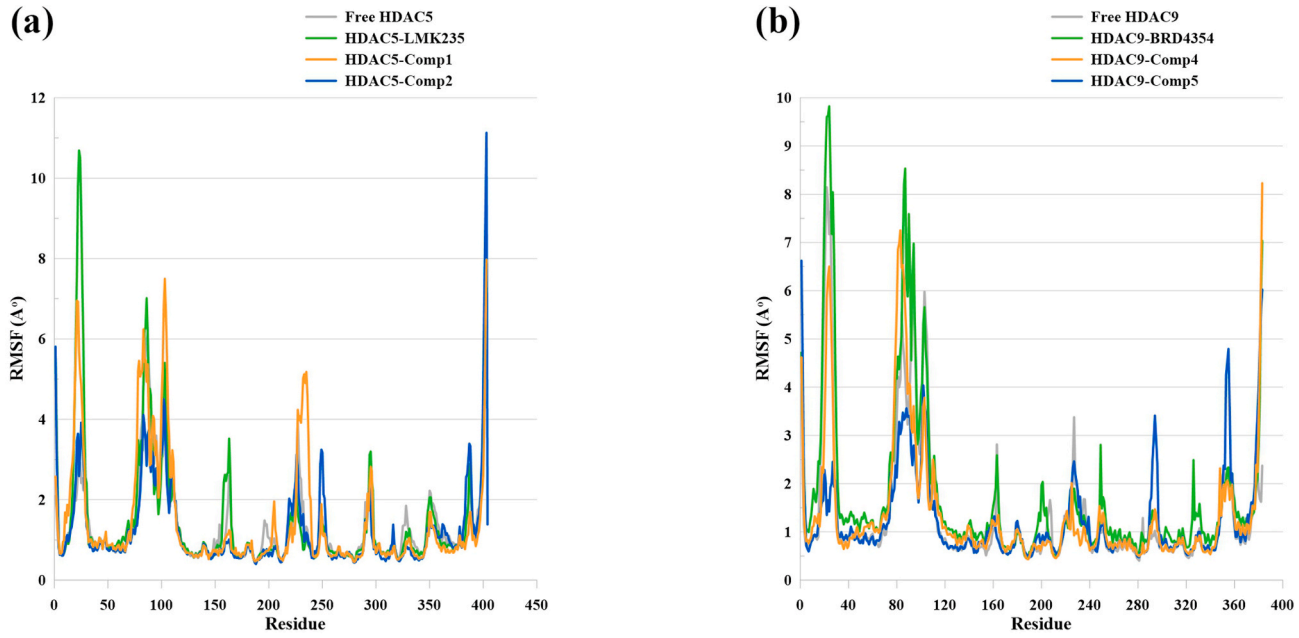

Fig. 7. Illustration of the root mean squared fluctuation (RMSF) for (a) HDAC5 complex systems; and (b) HDAC9 complex systems.

simulation and this observation agreed with the RMSD profiles of the same complex systems. The RMSF investigation showed that HDAC9-Comp5 displayed relatively lower amino acid residues fluctuations at major stable regions of the protein compared to the HDAC9-Comp4 system. This assessment was in agreement with the RMSD profiles of same complex systems.

3.5.3. Rg analysis

The protein compactness level can be examined via the radius of gyration (Rg) profile which is useful in investigating the protein folding nature throughout the simulation. The Rg of HDAC5 and its complex systems are plotted in Fig. 8 (a). All studied systems were remained stable over time. Compared to HDAC5-Comp1 system which has as average RMSF of 1.42 Å during the simulation, HDAC5-Comp2 system displayed lower Rg profile with a 1.27 Å, suggesting relatively less flexibility levels of the protein. The Rg profiles of HDAC9 systems implying that all complexes were steadily stable during the whole MD run (Fig. 8 (b)). HDAC9-Comp5 system exhibited a relatively higher degree of flexibility with an average Rg of 1.39 Å compared to HDAC9-Comp4 system that showed an average Rg of 1.26 Å during the simulation.

3.5.4. Potential energy analysis

Another useful measurement for examining the system stability over time is the potential energy profile. All studied systems were found to be stable and physically valid during MD simulations. HDAC5-Comp1 and HDAC5-Comp2 systems showed lower energy profiles compared to the apo-protein of HDAC5 and were found to be relatively similar to the energy of HDAC5-LMK235 complex system (Fig. 9 (a)). This observation was also noted in the HDAC9 complexes with the HDAC9-Comp4 and HDAC9-Comp5 systems, which displayed lower energy profiles than the apo-protein of HDAC9 (Fig. 9 (b)).

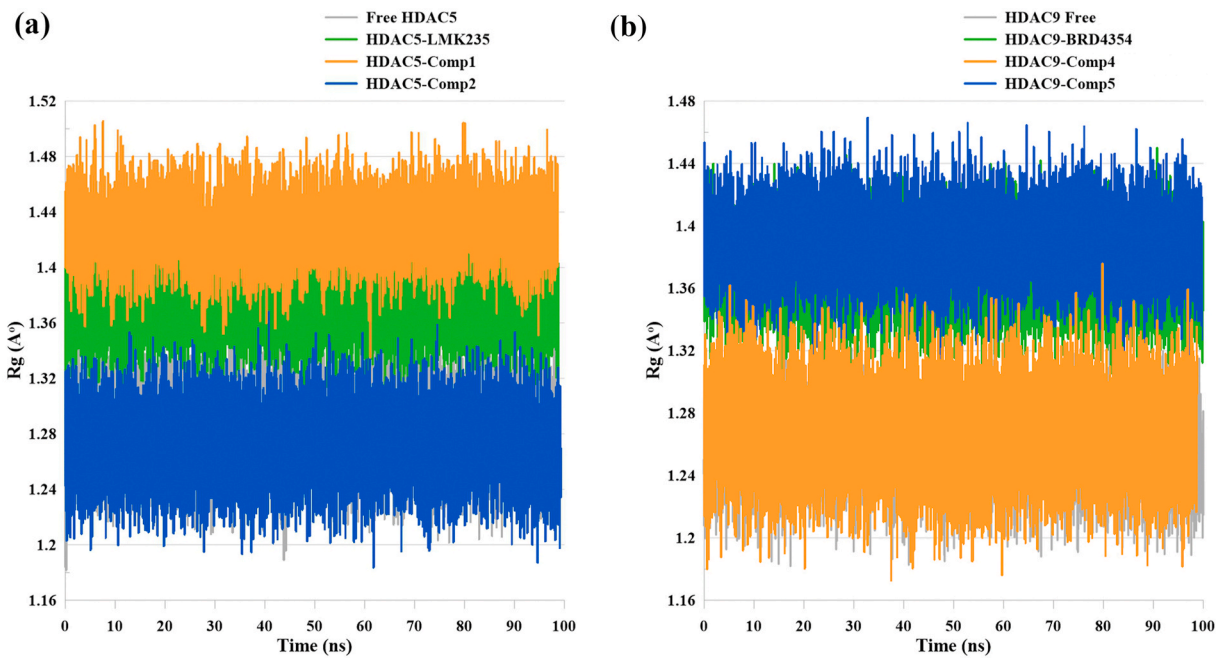

Fig. 8. Representation of the radius of gyration (Rg) for (a) HDAC5 complex systems; and (b) HDAC9 complex systems.

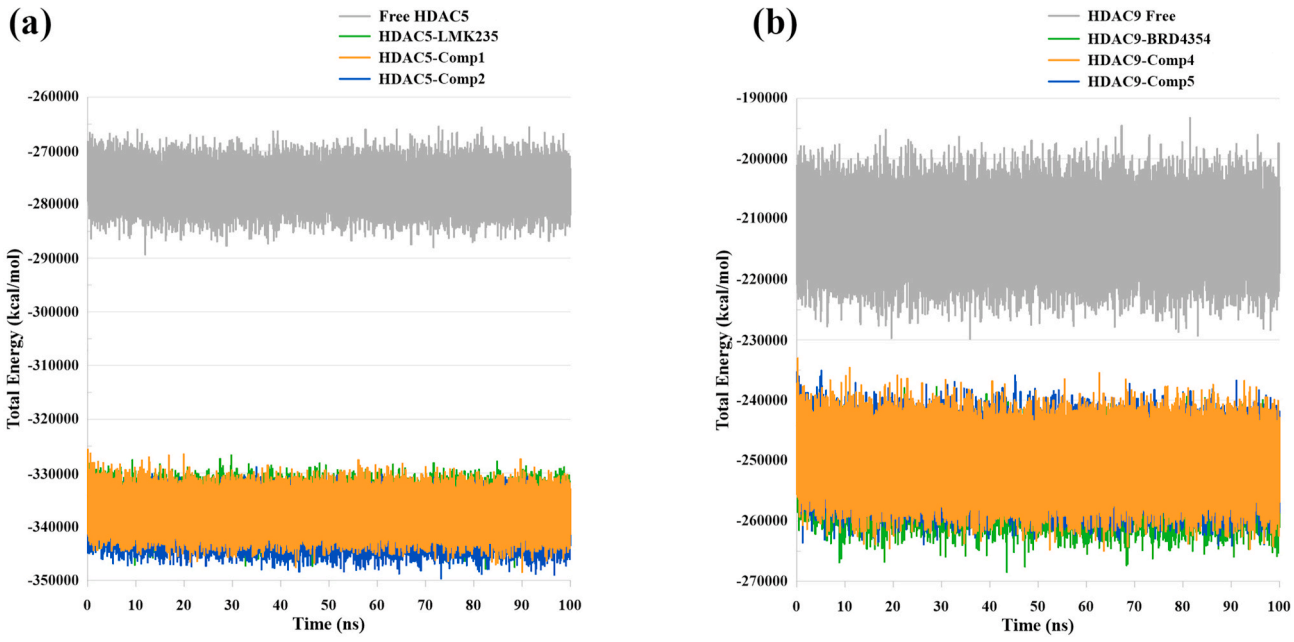

Fig. 9. Potential Energy profiles for (a) HDAC5 complex systems; and (b) HDAC9 complex systems.

3.5.5. Number of intermolecular hydrogen bonds

The binding affinity degree in protein-ligand complex is influenced by the number of hydrogen bonds and the more hydrogen bonds number the greater binding affinity level. HDAC5-Comp1 complex formed maximum of 4 H-bonds during the simulation (Fig. 10 (a)). The H-bond number gradually increased during the MD run especially after the first 50 ns. The maximum number of H-bonds formed in the HDAC5-Comp2 complex was found to be 5 (Fig. 10 (b)). The majority of the complex conformations were found to form 2 H-bonds. HDAC9-Comp5 complex formed at most 2 H-bonds in very few conformations while the average of the H-bonds was found to be 1 bond during the MD simulation (Fig. 10 (c)). Most of the conformations in HDAC9-Comp4 complex formed 1 H-bond throughout the simulation, and notably, the second half of the run showed an increased H-bond number with a maximum of 2 bonds (Fig. 10 (d)).

Throughout the 100 ns MD run, and in addition to the existence of water molecules, all studied systems showed good stability and the small molecules persisted their interaction with the active site of their corresponding targets. HDAC5-Comp2 complex was found to display overall lower RMSD trend than HDAC5-Comp1 complex. Whereas HDAC9 complex with Comp4 and Comp5 showed relatively similar RMSD profile.

3.5.6. MM-PBSA calculations

Free binding energy predictions employing MM-PBSA method has been successfully used to improve in silico predictions of ligand-protein

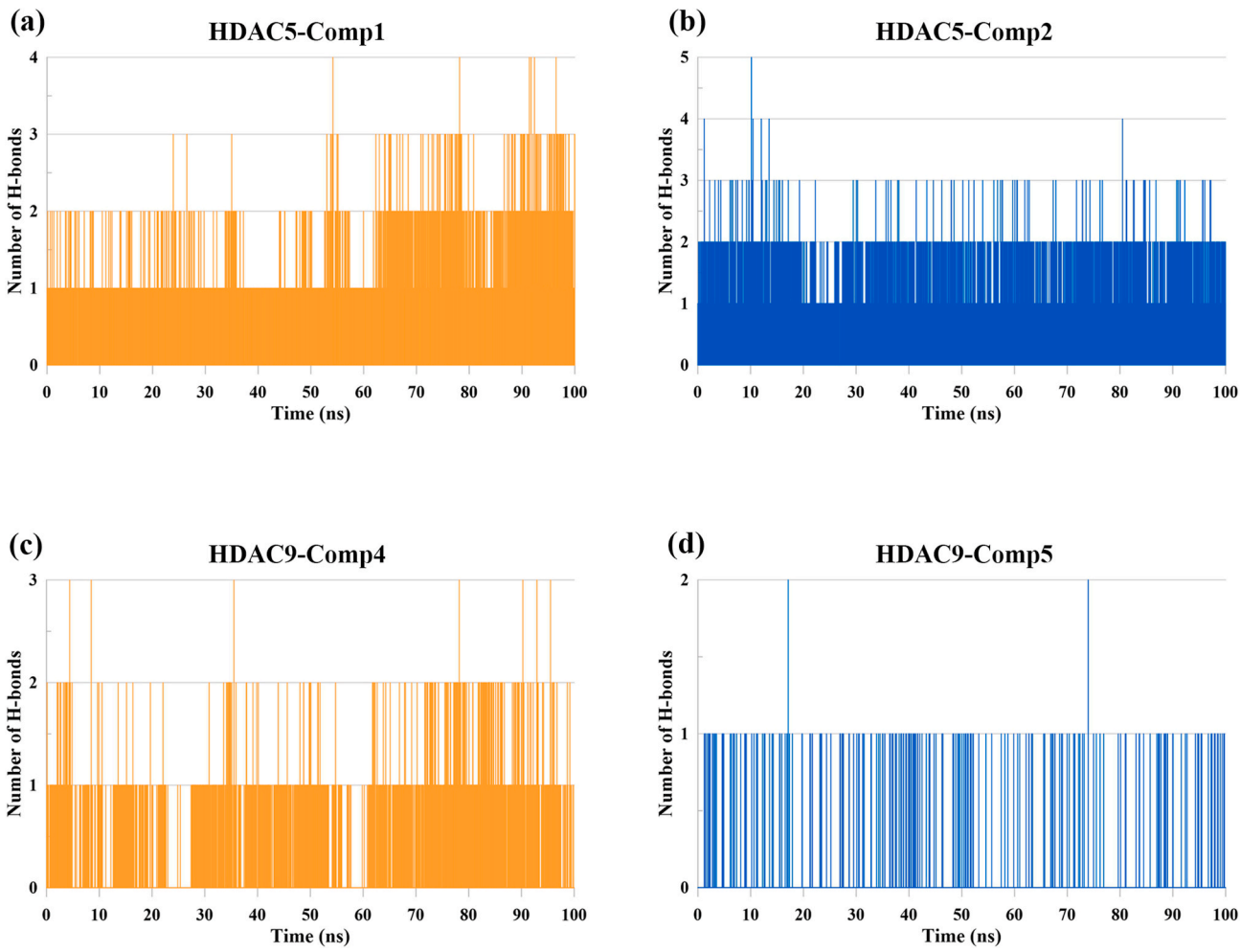

Fig. 10. Number of hydrogen bonds profile of (a) HDAC5-Comp1 complex; (b) HDAC5-Comp2 complex; (c) HDAC9-Comp4 complex; and (d) HDAC9-Comp5 complex.

affinity [141]. MM-PBSA method requires less exhaustive in silico calculations compared to QM/MM approaches [142,143]. In MM-PBSA calculations, nonpolar solvation energy, van der Waals, and electrostatic interactions negatively contribute to the total energy of the system, while positive contribution arises from polar solvation energy [144]. The average ΔG (binding free energy) of the four isoform selective compounds was computed for the last 10 ns applying the MM-PBSA approach. The MM-PBSA calculations showed an average ΔG of −19.67 ± 5.66 kcal/mol for the Comp1 -19.55 ± 5.08 kcal/mol for the Comp2; −18.85 ± 3.77 kcal/mol for the Comp4; and −16.11 ± 4.82 kcal/mol for the Comp5. Interestingly, the binding free energy calculations were found to be in good agreement with the QuickVina 2 rankings (Table 5). In addition, MM-PBSA calculations were performed for both reference known inhibitors, LMK235 and BRD4354. HDAC5-LMK235 displayed an average ΔG of −14.63 ± 7.83 kcal/mol, whereas the average ΔG for HDAC9-BRD4354 was found to be −14.33 5.97 kcal/mol. Therefore, MM-PBSA calculations of the 4 top-ranked compounds revealed lower binding energies and higher binding affinities toward their respective proteins compared to both reference compounds. According to the MM-PBSA calculations, the proposed compounds in the present study showed more negative energy compared to the QuickVina 2 binding energy calculations, suggesting the high affinity of the ligands to their respective targets.

4. Conclusion

To the best of our knowledge, although several efforts were made to discover novel HDACs inhibitors against several HDACs targets by pharmacophore modeling [145–147], our study is the first to apply this approach to identify novel and isoform-selective HDACs 5 and 9 inhibitors. In the current study, training and test sets composed of only HDACs inhibitors that are in clinical trials or with potential inhibition activity against HDACs 5 and 9. Due to the cytotoxicity accompanied by the use of several of the HDACs inhibitors that are already in clinical trials and uses, scientists around the world are paying more attention toward exploring isoform-selective inhibitors. Here, the HipHop module generated several pharmacophore hypotheses, where Hypo1 of HDAC5-pharmacophore was found to be the best model with an enrich factor of 10.26 and a goodness of hit (GH) of 0.86. Whereas Hypo2 of HDAC9-pharmacophore proved to be the most statistically satisfied model with an enrich factor of 10.13 and a goodness of hit (GH) of 0.87. Employing Hypo1 and Hypo2, the search for a novel potential inhibitors was achieved by the 3D database search using BIOVIA DS 4.5. Molecular docking study using QuickVina 2 has retrieved 3 potential selective inhibitors for HDAC5 and 3 for HDAC9. Comp1, Comp2, Comp4, and Comp5 showed good ADMET profile and demonstrated high binding mode stability during the 100 ns MD run. Proposed inhibitors could be used for further optimization as they showed potential isoform-selectivity toward HDAC5 and HDAC9. Hence, further details about the structural features essential for identifying HDACs 5 and 9

selective inhibitors may be offered by the present study, providing opportunities for additional computational (in silico) and in vitro experiments in order to enhance the selectivity and potency of the proposed inhibitors.

Declaration of competing interest

The authors declare that they have no known competing financial interests or personal relationships that could have appeared to influence the work reported in this paper.

Acknowledgments

Authors would like to thank the Directorate of Research and Development Resources of Kadir Has University.

Appendix A. Supplementary data

Supplementary data to this article can be found online at https://doi.org/10.1016/j.jmgm.2021.107937.

Funding sources

This research did not receive any specific grant from funding agencies in the public, commercial, or not-for-profit sectors.

Author contributions statement

ADE and KY conceived the experiment(s); ADE and AA conducted the experiment(s); ADE and KY analyzed the results; ADE drafted the manuscript; KY proofread and reviewed the manuscript.

Data availability

All data created or examined in this work are included in this article.

References

[1] J. Casadesús, M. Noyer-Weidner, K.B.T.-B.E. of G. (Second E. Hughes, Epigenetics, in: S. Maloy (Ed.), Brenner's Encycl. Genet, second ed., Academic Press, San Diego, 2013 https://doi.org/10.1016/B978-0-12-374984-0.00480-0, 500–503.

[2] S.K. Agarwal, L.S. Weinstein, Genetics of Bone Biology and Skeletal Disease (Second Edition), in: R.V. Thakker, M.P. Whyte, J.A. Eisman, T. Igarashi (Eds.), Chapter 2 - Epigenetics, Academic Press, 2018, pp. 25–32, https://doi.org/10.1016/B978-0-12-804182-6.00002-2.

[3] T.G. Bredfeldt, C.L. Walker, Epigenetics, in: C.A.B.T.-C.T. (Second E. McQueen (Ed.), Compr. Toxicol, second ed., Elsevier, Oxford, 2010, pp. 335–358, https://doi.org/10.1016/B978-0-08-046884-6.00219-0.

[4] E.L. Mersfelder, M.R. Parthun, The tale beyond the tail: histone core domain modifications and the regulation of chromatin structure, Nucleic Acids Res. 34 (2006) 2653–2662, https://doi.org/10.1093/nar/gkl338.

[5] G. Milazzo, D. Mercatelli, G. Di Muzio, L. Triboli, P. De Rosa, G. Perini, F. M. Giorgi, Histone deacetylases (HDACs): evolution, specificity, role in transcriptional complexes, and pharmacological actionability, Genes 11 (2020) 556, https://doi.org/10.3390/genes11050556.

[6] C. Choudhary, C. Kumar, F. Gnad, M.L. Nielsen, M. Rehman, T.C. Walther, J. V. Olsen, M. Mann, Lysine acetylation targets protein complexes and co-regulates major cellular functions, Science (80-.) 325 (2009) 834–840, https://doi.org/10.1126/science.1175371.

[7] X.J. Yang, E. Seto, The Rpd3/Hda1 family of lysine deacetylases: from bacteria and yeast to mice and men, Nat. Rev. Mol. Cell Biol. 9 (2008) 206–218, https://doi.org/10.1038/nrm2346.

[8] P.A. Marks, W.S. Xu, Histone deacetylase inhibitors: potential in cancer therapy, J. Cell. Biochem. 107 (2009) 600–608, https://doi.org/10.1002/jcb.22185.

[9] S.I. Imai, C.M. Armstrong, M. Kaeberlein, L. Guarente, Transcriptional silencing and longevity protein Sir2 is an NAD-dependent histone deacetylase, Nature 403 (2000) 795–800, https://doi.org/10.1038/35001622.

[10] B. Barneda-Zahonero, M. Parra, Histone deacetylases and cancer, Mol. Oncol. 6 (2012) 579–589, https://doi.org/10.1016/j.molonc.2012.07.003.

[11] M. Haberland, R.L. Montgomery, E.N. Olson, The many roles of histone deacetylases in development and physiology: implications for disease and therapy, Nat. Rev. Genet. 10 (2009) 32–42, https://doi.org/10.1038/nrg2485.

[12] C.M. Grozinger, S.L. Schreiber, Regulation of histone deacetylase 4 and 5 and transcriptional activity by 14-3-3-dependent cellular localization, Proc. Natl. Acad. Sci. U.S.A. 97 (2000) 7835–7840, https://doi.org/10.1073/pnas.140199597.

[13] H.G. Kasler, E. Verdin, The class IIa histone deacetylases, in: E. Verdin (Ed.), Histone Deacetylases, Humana Press, Totowa, NJ, 2006, pp. 129–163, https://doi.org/10.1385/1-59745-024-3, 129.

[14] A.J.M. De Ruijter, A.H. Van Gennip, H.N. Caron, S. Kemp, A.B.P. Van Kuilenburg, Histone deacetylases (HDACs): characterization of the classical HDAC family, Biochem. J. 370 (2003) 737–749, https://doi.org/10.1042/BJ20021321.

[15] A. Schuetz, J. Min, A. Allali-Hassani, M. Schapira, M. Shuen, P. Loppnau, R. Mazitschek, N.P. Kwiatkowski, T.A. Lewis, R.L. Maglathin, T.H. McLean, A. Bochkarev, A.N. Plotnikov, M. Vedadi, C.H. Arrowsmith, Human HDAC7 harbors a class IIa histone deacetylase-specific zinc binding motif and cryptic deacetylase activity, J. Biol. Chem. 283 (2008) 11355–11363, https://doi.org/10.1074/jbc.M707362200.

[16] A. Lahm, C. Paolini, M. Pallaoro, M.C. Nardi, P. Jones, P. Neddermann, S. Sambucini, M.J. Bottomley, P. Lo Surdo, A. Carfí, U. Koch, R. De Francesco, C. Steinkühler, P. Gallinari, Unraveling the hidden catalytic activity of vertebrate class IIa histone deacetylases, Proc. Natl. Acad. Sci. U.S.A. 104 (2007) 17335–17340, https://doi.org/10.1073/pnas.0706487104.

[17] M.J. Bottomley, P. Lo Lo Surdo, P. Di Di Giovine, A. Cirillo, R. Scarpelli, F. Ferrigno, P. Jones, P. Neddermann, R. De Francesco, C. Steinkühler, P. Gallinari, A. Carfí, Structural and functional analysis of the human HDAC4 catalytic domain reveals a regulatory structural zinc-binding domain, J. Biol. Chem. 283 (2008) 26694–26704, https://doi.org/10.1074/jbc.M803514200.

[18] R.W. Bürli, C.A. Luckhurst, O. Aziz, K.L. Matthews, D. Yates, K.A. Lyons, M. Beconi, G. McAllister, P. Breccia, A.J. Stott, S.D. Penrose, M. Wall, M. Lamers, P. Leonard, I. Müller, C.M. Richardson, R. Jarvis, L. Stones, S. Hughes, G. Wishart, A.F. Haughan, C. O'Connell, T. Mead, H. McNeil, J. Vann, J. Mangette, M. Maillard, V. Beaumont, I. Munoz-Sanjuan, C. Dominguez, Design, synthesis, and biological evaluation of potent and selective class IIa histone deacetylase (HDAC) inhibitors as a potential therapy for huntington's disease, J. Med. Chem. 56 (2013) 9934–9954, https://doi.org/10.1021/jm4011884.

[19] S.L. McGee, B.J.W. Van Denderen, K.F. Howlett, J. Mollica, J.D. Schertzer, B. E. Kemp, M. Hargreaves, AMP-activated protein kinase regulates GLUT4 transcription by phosphorylating histone deacetylase 5, Diabetes 57 (2008) 860–867, https://doi.org/10.2337/db07-0843.

[20] V. Moresi, N. Marroncelli, D. Coletti, S. Adamo, Regulation of skeletal muscle development and homeostasis by gene imprinting, histone acetylation and microRNA, Biochim. Biophys. Acta - Gene Regul. Mech. 1849 (2015) 309–316, https://doi.org/10.1016/j.bbagrm.2015.01.002.

[21] B. Lang, T.M.A. Alrahbeni, D.S. Clair, D.H. Blackwood, I.S. Consortium, C. D. McCaig, S. Shen, HDAC9 is implicated in schizophrenia and expressed specifically in post-mitotic neurons but not in adult neural stem cells, Am. J. Stem Cells. 1 (2011) 31–41. https://pubmed.ncbi.nlm.nih.gov/23671795.

[22] R.E. Schmieder, F.H. Messerli, G.E. Garavaglia, B.D. Nunez, Dietary salt intake: a determinant of cardiac involvement in essential hypertension, Circulation 78 (1988) 951–956, https://doi.org/10.1161/01.CIR.78.4.951.

[23] S. Popov, K. Venetsanou, P. Jorge Chedrese, V. Pinto, H. Takemori, A. Franco-Cereceda, P. Eriksson, N. Mochizuki, P. Soares-da-Silva, A.M. Bertorello, Increases in intracellular sodium activate transcription and gene expression via the salt-inducible kinase 1 network in an atrial myocyte cell line, Am. J. Physiol. Heart Circ. Physiol. 303 (2012), https://doi.org/10.1152/ajpheart.00512.2011. H57–H65.

[24] E.D. Frohlich, Y. Chien, S. Sesoko, B.L. Pegram, Relationship between dietary sodium intake, hemodynamics, and cardiac mass in SHR and WKY rats, Am. J. Physiol. Regul. Integr. Comp. Physiol. 264 (1993), https://doi.org/10.1152/ajpregu.1993.264.1.r30. R30–R34.

[25] S. Ropero, M. Esteller, The role of histone deacetylases (HDACs) in human cancer, Mol. Oncol. 1 (2007) 19–25, https://doi.org/10.1016/j.molonc.2007.01.001.

[26] L. Zhong, S. Sun, S. Yao, X. Han, M. Gu, J. Shi, Histone deacetylase 5 promotes the proliferation and invasion of lung cancer cells, Oncol. Rep. 40 (2018) 2224–2232, https://doi.org/10.3892/or.2018.6591.

[27] Y. Huang, M. Tan, M. Gosink, K.K.W. Wang, Y. Sun, Histone deacetylase 5 is not a p53 target gene, but its overexpression inhibits tumor cell growth and induces apoptosis, Canc. Res. 62 (2002) 2913–2922. http://cancerres.aacrjournals.org/content/62/10/2913.abstract.

[28] D.A. Moreno, C.A. Scrideli, M.A.A. Cortez, R. De Paula Queiroz, E.T. Valera, V. Da Silva Silveira, J.A. Yunes, S.R. Brandalise, L.G. Tone, Differential expression of HDAC3, HDAC7 and HDAC9 is associated with prognosis and survival in childhood acute lymphoblastic leukaemia: research paper, Br. J. Haematol. 150 (2010) 665–673, https://doi.org/10.1111/j.1365-2141.2010.08301.x.

[29] A. Clocchiatti, E. Di Giorgio, S. Ingrao, F.J. Meyer-Almes, C. Tripodo, C. Brancolini, Class IIa HDACs repressive activities on MEF2-depedent transcription are associated with poor prognosis of ER+ breast tumors, Faseb. J. 27 (2013) 942–954, https://doi.org/10.1096/fj.12-209346.

[30] Y.X. Zhao, Y.S. Wang, Q.Q. Cai, J.Q. Wang, W.T. Yao, Up-regulation of HDAC9 promotes cell proliferation through suppressing p53 transcription in osteosarcoma, Int. J. Clin. Exp. Med. 8 (2015) 11818–11823. https://pubmed.ncbi.nlm.nih.gov/26380023.

[31] M. Lapierre, A. Linares, M. Dalvai, C. Duraffourd, S. Bonnet, A. Boulahtouf, C. Rodriguez, S. Jalaguier, S. Assou, B. Orsetti, P. Balaguer, T. Maudelonde, P. Blache, K. Bystricky, N. Boulle, V. Cavaillès, Histone deacetylase 9 regulates breast cancer cell proliferation and the response to histone deacetylase inhibitors, Oncotarget 7 (2016), https://doi.org/10.18632/oncotarget.7564, 19693–19708.

[32] V.S. Gil, G. Bhagat, L. Howell, J. Zhang, C.H. Kim, S. Stengel, F. Vega, A. Zelent, K. Petrie, Deregulated expression of HDAC9 in B cells promotes development of lymphoproliferative disease and lymphoma in mice, DMM Dis. Model. Mech. 9 (2016) 1483–1495, https://doi.org/10.1242/dmm.023366.
[33] E.E. Hull, M.R. Montgomery, K.J. Leyva, HDAC inhibitors as epigenetic regulators of the immune system: impacts on cancer therapy and inflammatory diseases, BioMed Res. Int. 2016 (2016) 8797206, https://doi.org/10.1155/2016/8797206.
[34] T. Eckschlager, J. Plch, M. Stiborova, J. Hrabeta, Histone deacetylase inhibitors as anticancer drugs, Int. J. Mol. Sci. 18 (2017), https://doi.org/10.3390/ijms18071414.
[35] H.J. Kim, S.C. Bae, Histone deacetylase inhibitors: molecular mechanisms of action and clinical trials as anti-cancer drugs, Am. J. Transl. Res. 3 (2011) 166–179. https://pubmed.ncbi.nlm.nih.gov/21416059.
[36] M. Jung, Inhibitors of histone deacetylase as new anticancer agents, Curr. Med. Chem. 8 (2012) 1505–1511, https://doi.org/10.2174/0929867013372058.
[37] M. Jung, G. Brosch, D. Kölle, H. Scherf, C. Gerhäuser, P. Loidl, Amide analogues of trichostatin A as inhibitors of histone deacetylase and inducers of terminal cell differentiation, J. Med. Chem. 42 (1999) 4669–4679, https://doi.org/10.1021/jm991091h.
[38] M.S. Finnin, J.R. Donigian, A. Cohen, V.M. Richon, R.A. Rifkind, P.A. Marks, R. Breslow, N.P. Pavletich, Structures of a histone deacetylase homologue bound to the TSA and SAHA inhibitors, Nature 401 (1999) 188–193, https://doi.org/10.1038/43710.
[39] J. Melesina, L. Praetorius, C.V. Simoben, D. Robaa, W. Sippl, Design of selective histone deacetylase inhibitors: rethinking classical pharmacophore, Future Med. Chem. 10 (2018) 1537–1540, https://doi.org/10.4155/fmc-2018-0125.
[40] M. Mottamal, S. Zheng, T.L. Huang, G. Wang, Histone deacetylase inhibitors in clinical studies as templates for new anticancer agents, Molecules 20 (2015) 3898–3941, https://doi.org/10.3390/molecules20033898.
[41] D.C. Drummond, C.O. Noble, D.B. Kirpotin, Z. Guo, G.K. Scott, C.C. Benz, Clinical development of histone deacetylase inhibitors as anticancer agents, Annu. Rev. Pharmacol. Toxicol. 45 (2005) 495–528, https://doi.org/10.1146/annurev.pharmtox.45.120403.095825.
[42] J.E. Bolden, M.J. Peart, R.W. Johnstone, Anticancer activities of histone deacetylase inhibitors, Nat. Rev. Drug Discov. 5 (2006) 769–784, https://doi.org/10.1038/nrd2133.
[43] S.B. Nair, M.K. Teli, H. Pradeep, G.K. Rajanikant, Computational identification of novel histone deacetylase inhibitors by docking based QSAR, Comput, Biol. Med. 42 (2012) 697–705, https://doi.org/10.1016/j.compbiomed.2012.04.001.
[44] B.S. Mann, J.R. Johnson, M.H. Cohen, R. Justice, R. Pazdur, FDA approval summary: Vorinostat for treatment of advanced primary cutaneous T-cell lymphoma, Oncol. 12 (2007) 1247–1252, https://doi.org/10.1634/theoncologist.12-10-1247.
[45] C. Schölz, B.T. Weinert, S.A. Wagner, P. Beli, Y. Miyake, J. Qi, L.J. Jensen, W. Streicher, A.R. McCarthy, N.J. Westwood, S. Lain, J. Cox, P. Matthias, M. Mann, J.E. Bradner, C. Choudhary, Acetylation site specificities of lysine deacetylase inhibitors in human cells, Nat. Biotechnol. 33 (2015) 415–425, https://doi.org/10.1038/nbt.3130.
[46] L. Ellis, R. Pili, Histone deacetylase inhibitors: advancing therapeutic strategies in hematological and solid malignancies, Pharmaceuticals 3 (2010) 2441–2469, https://doi.org/10.3390/ph3082441.
[47] M. Bantscheff, C. Hopf, M.M. Savitski, A. Dittmann, P. Grandi, A.M. Michon, J. Schlegl, Y. Abraham, I. Becher, G. Bergamini, M. Boesche, M. Delling, B. Dümpelfeld, D. Eberhard, C. Huthmacher, T. Mathieson, D. Poeckel, V. Reader, K. Strunk, G. Sweetman, U. Kruse, G. Neubauer, N.G. Ramsden, G. Drewes, Chemoproteomics profiling of HDAC inhibitors reveals selective targeting of HDAC complexes, Nat. Biotechnol. 29 (2011) 255–268, https://doi.org/10.1038/nbt.1759.
[48] H.Z. Lee, V.E. Kwitkowski, P.L. Del Valle, M.S. Ricci, H. Saber, B.A. Habtemariam, J. Bullock, E. Bloomquist, Y.L. Shen, X.H. Chen, J. Brown, N. Mehrotra, S. Dorff, R. Charlab, R.C. Kane, E. Kaminskas, R. Justice, A.T. Farrell, R. Pazdur, FDA approval: belinostat for the treatment of patients with relapsed or refractory peripheral T-cell lymphoma, Clin. Canc. Res. 21 (2015) 2666–2670, https://doi.org/10.1158/1078-0432.CCR-14-3119.
[49] J.P. Laubach, P. Moreau, J.F. San-Miguel, P.G. Richardson, Panobinostat for the treatment of multiple myeloma, Clin. Canc. Res. 21 (2015) 4767–4773, https://doi.org/10.1158/1078-0432.CCR-15-0530.
[50] A. Olsson, A. Björk, J. Vallon-Christersson, J.T. Isaacs, T. Leanderson, Tasquinimod (ABR-215050), a quinoline-3-carboxamide anti-angiogenic agent, modulates the expression of thrombospondin-1 in human prostate tumors, Mol. Canc. 9 (2010) 107, https://doi.org/10.1186/1476-4598-9-107.
[51] J.T. Isaacs, L. Antony, S.L. Dalrymple, W.N. Brennen, S. Gerber, H. Hammers, M. Wissing, S. Kachhap, J. Luo, L. Xing, P. Bjork, A. Olsson, A. Bjork, T. Leanderson, Tasquinimod is an allosteric modulator of HDAC4 survival signaling within the compromised cancer microenvironment, Canc. Res. 73 (2013) 1386–1399, https://doi.org/10.1158/0008-5472.CAN-12-2730.
[52] S.L. Dalrymple, R.E. Becker, H. Zhou, T.L. Deweese, J.T. Isaacs, Tasquinimod prevents the angiogenic rebound induced by fractionated radiation resulting in an enhanced therapeutic response of prostate cancer xenografts, Prostate 72 (2012) 638–648, https://doi.org/10.1002/pros.21467.
[53] I. Venza, M. Visalli, R. Oteri, M. Cucinotta, D. Teti, M. Venza, Class II-specific histone deacetylase inhibitors MC1568 and MC1575 suppress IL-8 expression in human melanoma cells, Pigment Cell Melanoma Res 26 (2013) 193–204, https://doi.org/10.1111/pcmr.12049.
[54] A. Nebbioso, C. Dell'Aversana, A. Bugge, R. Sarno, S. Valente, D. Rotili, F. Manzo, D. Teti, S. Mandrup, P. Ciana, A. Maggi, A. Mai, H. Gronemeyer, L. Altucci, HDACs class II-selective inhibition alters nuclear receptor-dependent differentiation, J. Mol. Endocrinol. 45 (2010) 219–228, https://doi.org/10.1677/JME-10-0043.
[55] A. Mai, S. Massa, R. Pezzi, S. Simeoni, D. Rotili, A. Nebbioso, A. Scognamiglio, L. Altucci, P. Loidl, G. Brosch, Class II (IIa)-selective histone deacetylase inhibitors. 1. Synthesis and biological evaluation of novel (aryloxopropenyl) pyrrolyl hydroxyamides, J. Med. Chem. 48 (2005) 3344–3353, https://doi.org/10.1021/jm049002a.
[56] V. Duong, C. Bret, L. Altucci, A. Mai, C. Duraffourd, J. Loubersac, P.O. Harmand, S. Bonnet, S. Valente, T. Maudelonde, V. Cavailles, N. Boulle, Specific activity of class II histone deacetylases in human breast cancer cells, Mol. Canc. Res. 6 (2008) 1908–1919, https://doi.org/10.1158/1541-7786.MCR-08-0299.
[57] L. Marek, A. Hamacher, F.K. Hansen, K. Kuna, H. Gohlke, M.U. Kassack, T. Kurz, Histone deacetylase (HDAC) inhibitors with a novel connecting unit linker region reveal a selectivity profile for HDAC4 and HDAC5 with improved activity against chemoresistant cancer cells, J. Med. Chem. 56 (2013) 427–436, https://doi.org/10.1021/jm301254q.
[58] M. Lobera, K.P. Madauss, D.T. Pohlhaus, Q.G. Wright, M. Trocha, D.R. Schmidt, E. Baloglu, R.P. Trump, M.S. Head, G.A. Hofmann, M. Murray-Thompson, B. Schwartz, S. Chakravorty, Z. Wu, P.K. Mander, L. Kruidenier, R.A. Reid, W. Burkhart, B.J. Turunen, J.X. Rong, C. Wagner, M.B. Moyer, C. Wells, X. Hong, J.T. Moore, J.D. Williams, D. Soler, S. Ghosh, M.A. Nolan, Selective class IIa histone deacetylase inhibition via a nonchelating zinc-binding group, Nat. Chem. Biol. 9 (2013) 319–325, https://doi.org/10.1038/nchembio.1223.
[59] Z.V. Boskovic, M.M. Kemp, A.M. Freedy, V.S. Viswanathan, M.S. Pop, J.H. Fuller, N.M. Martinez, S.O. Figueroa Lazú, J.A. Hong, T.A. Lewis, D. Calarese, J.D. Love, A. Vetere, S.C. Almo, S.L. Schreiber, A.N. Koehler, Inhibition of zinc-dependent histone deacetylases with a chemically triggered electrophile, ACS Chem. Biol. 11 (2016) 1844–1851, https://doi.org/10.1021/acschembio.6b00012.
[60] P. Jones, M.J. Bottomley, A. Carfí, O. Cecchetti, F. Ferrigno, P. Lo Surdo, J. M. Ontoria, M. Rowley, R. Scarpelli, C. Schultz-Fademrecht, C. Steinkühler, 2-Trifluoroacetylthiophenes, a novel series of potent and selective class II histone deacetylase inhibitors, Bioorg. Med. Chem. Lett 18 (2008) 3456–3461, https://doi.org/10.1016/j.bmcl.2008.02.026.
[61] C.A. Luckhurst, O. Aziz, V. Beaumont, R.W. Bürli, P. Breccia, M.C. Maillard, A. F. Haughan, M. Lamers, P. Leonard, K.L. Matthews, G. Raphy, A.J. Stott, I. Munoz-Sanjuan, B. Thomas, M. Wall, G. Wishart, D. Yates, C. Dominguez, Development and characterization of a CNS-penetrant benzhydryl hydroxamic acid class IIa histone deacetylase inhibitor, Bioorg. Med. Chem. Lett 29 (2019) 83–88, https://doi.org/10.1016/j.bmcl.2018.11.009.
[62] S.R. Langdon, P. Ertl, N. Brown, Bioisosteric replacement and scaffold hopping in lead generation and optimization, Mol. Inform. 29 (2010) 366–385, https://doi.org/10.1002/minf.201000019.
[63] T. Wang, M. Sepulveda, P. Gonzales, S. Gately, Identification of novel HDAC inhibitors through cell based screening and their evaluation as potential anticancer agents, Bioorg. Med. Chem. Lett 23 (2013) 4790–4793, https://doi.org/10.1016/j.bmcl.2013.07.001.
[64] H. Park, S. Kim, Y.E. Kim, S.J. Lim, A structure-based virtual screening approach toward the discovery of histone deacetylase inhibitors: identification of promising zinc-chelating groups, ChemMedChem 5 (2010) 591–597, https://doi.org/10.1002/cmdc.200900500.
[65] Y. xin Huang, J. Zhao, Q. hang Song, L. hua Zheng, C. Fan, T. ting Liu, Y. li Bao, L. guo Sun, L. biao Zhang, Y. xin Li, Virtual screening and experimental validation of novel histone deacetylase inhibitors, BMC Pharmacol. Toxicol. 17 (2016) 32, https://doi.org/10.1186/s40360-016-0075-8.
[66] Y. dong Chen, Y.J. Jiang, J.W. Zhou, Q. Sen Yu, Q.D. You, Identification of ligand features essential for HDACs inhibitors by pharmacophore modeling, J. Mol. Graph. Model. 26 (2008) 1160–1168, https://doi.org/10.1016/j.jmgm.2007.10.007.
[67] S.Y. Yang, Pharmacophore modeling and applications in drug discovery: challenges and recent advances, Drug Discov. Today 15 (2010) 444–450, https://doi.org/10.1016/j.drudis.2010.03.013.
[68] C.G. Wermuth, C.R. Ganellin, P. Lindberg, L.A. Mitscher, Glossary of terms used in medicinal chemistry (IUPAC Recommendations 1998), Pure Appl. Chem. 70 (1998) 1129–1143, https://doi.org/10.1351/pac199870051129.
[69] A.D. Elmezayen, K. Yelekçi, Homology modeling and in silico design of novel and potential dual-acting inhibitors of human histone deacetylases HDAC5 and HDAC9 isozymes, J. Biomol. Struct. Dyn. (2020) 1–19, https://doi.org/10.1080/07391102.2020.1798812.
[70] Dassault Systèmes, BIOVIA Discovery Studio Visualizer, 2016. V16.1.0.15350.
[71] A. Gaulton, A. Hersey, M.L. Nowotka, A. Patricia Bento, J. Chambers, D. Mendez, P. Mutowo, F. Atkinson, L.J. Bellis, E. Cibrian-Uhalte, M. Davies, N. Dedman, A. Karlsson, M.P. Magarinos, J.P. Overington, G. Papadatos, I. Smit, A.R. Leach, The ChEMBL database in 2017, Nucleic Acids Res. 45 (2017) D945–D954, https://doi.org/10.1093/nar/gkw1074.
[72] R. De Vreese, M. D'hooghe, Synthesis and applications of benzohydroxamic acid-based histone deacetylase inhibitors, Eur. J. Med. Chem. 135 (2017) 174–195, https://doi.org/10.1016/j.ejmech.2017.04.013.
[73] G. Giannini, M. Marzi, M. Di Marzo, G. Battistuzzi, R. Pezzi, T. Brunetti, W. Cabri, L. Vesci, C. Pisano, Exploring bis-(indolyl)methane moiety as an alternative and innovative CAP group in the design of histone deacetylase (HDAC) inhibitors, Bioorg. Med. Chem. Lett 19 (2009) 2840–2843, https://doi.org/10.1016/j.bmcl.2009.03.101.
[74] G. Giannini, M. Marzi, R. Pezzi, T. Brunetti, G. Battistuzzi, M. Di Marzo, W. Cabri, L. Vesci, C. Pisano, N-Hydroxy-(4-oxime)-cinnamide: a versatile scaffold for the

synthesis of novel histone deacetilase (HDAC) inhibitors, Bioorg. Med. Chem. Lett 19 (2009) 2346–2349, https://doi.org/10.1016/j.bmcl.2009.02.029.
[75] D.M. Hutt, D. Herman, A.P.C. Rodrigues, S. Noel, J.M. Pilewski, J. Matteson, B. Hoch, W. Kellner, J.W. Kelly, A. Schmidt, P.J. Thomas, Y. Matsumura, W. R. Skach, M. Gentzsch, J.R. Riordan, E.J. Sorscher, T. Okiyoneda, J.R. Yates, G. L. Lukacs, R.A. Frizzell, G. Manning, J.M. Gottesfeld, W.E. Balch, Reduced histone deacetylase 7 activity restores function to misfolded CFTR in cystic fibrosis, Nat. Chem. Biol. 6 (2010) 25–33, https://doi.org/10.1038/nchembio.275.
[76] J.H. Kalin, J.A. Bergman, Development and therapeutic implications of selective histone deacetylase 6 inhibitors, J. Med. Chem. 56 (2013) 6297–6313, https://doi.org/10.1021/jm4001659.
[77] K.S. Ko, M.E. Steffey, K.R. Brandvold, M.B. Soellner, Development of a chimeric c-Src kinase and HDAC inhibitor, ACS Med. Chem. Lett. 4 (2013) 779–783, https://doi.org/10.1021/ml400175d.
[78] H.Y. Lee, J.F. Lee, S. Kumar, Y.W. Wu, W.C. HuangFu, M.J. Lai, Y.H. Li, H. L. Huang, F.C. Kuo, C.J. Hsiao, C.C. Cheng, C.R. Yang, J.P. Liou, 3-Aroylindoles display antitumor activity in vitro and in vivo: effects of N1-substituents on biological activity, Eur. J. Med. Chem. 125 (2017) 1268–1278, https://doi.org/10.1016/j.ejmech.2016.11.033.
[79] D.E. Olson, F.F. Wagner, T. Kaya, J.P. Gale, N. Aidoud, E.L. Davoine, F. Lazzaro, M. Weïwer, Y.L. Zhang, E.B. Holson, Discovery of the first histone deacetylase 6/8 dual inhibitors, J. Med. Chem. 56 (2013) 4816–4820, https://doi.org/10.1021/jm400390r.
[80] M. Paris, M. Porcelloni, M. Binaschi, D. Fattori, Histone deacetylase inhibitors: from bench to clinic, J. Med. Chem. 51 (2008) 1505–1529, https://doi.org/10.1021/jm7011408.
[81] G. Pescatore, O. Kinzel, B. Attenni, O. Cecchetti, F. Fiore, M. Fonsi, M. Rowley, C. Schultz-Fademrecht, S. Serafini, C. Steinkühler, P. Jones, Optimization of a series of potent and selective ketone histone deacetylase inhibitors, Bioorg. Med. Chem. Lett 18 (2008) 5528–5532, https://doi.org/10.1016/j.bmcl.2008.09.003.
[82] S. Raeppel, N. Zhou, F. Gaudette, S. Leit, I. Paquin, G. Larouche, O. Moradei, S. Fréchette, L. Isakovic, D. Delorme, M. Fournel, A. Kalita, A. Lu, M.C. Trachy-Bourget, P.T. Yan, J. Liu, J. Rahil, J. Wang, J.M. Besterman, K. Murakami, Z. Li, A. Vaisburg, SAR and biological evaluation of analogues of a small molecule histone deacetylase inhibitor N-(2-aminophenyl)-4-((4-(pyridin-3-yl)pyrimidin-2-ylamino)methyl)benzamide (MGCD0103), Bioorg. Med. Chem. Lett 19 (2009) 644–649, https://doi.org/10.1016/j.bmcl.2008.12.048.
[83] H. Sekizawa, K. Amaike, Y. Itoh, T. Suzuki, K. Itami, J. Yamaguchi, Late-stage C-H coupling enables rapid identification of HDAC inhibitors: synthesis and evaluation of NCH-31 analogues, ACS Med. Chem. Lett. 5 (2014) 582–586, https://doi.org/10.1021/ml500024s.
[84] C.D.T. Stephen Joseph Shuttleworth, Shuttleworth, Scriptaid Isosteres and Their Use in Therapy, US8748458B2, 2014. https://patents.google.com/patent/US8748458B2/en?oq=8748458.
[85] F.F. Wagner, D.E. Olson, J.P. Gale, T. Kaya, M. Weïwer, N. Aidoud, M. Thomas, E. L. Davoine, B.C. Lemercier, Y.L. Zhang, E.B. Holson, Potent and selective inhibition of histone deacetylase 6 (HDAC6) does not require a surface-binding motif, J. Med. Chem. 56 (2013) 1772–1776, https://doi.org/10.1021/jm301355j.
[86] H.W. Ziwei Yun, Yun, Quinolyl-containing Hydroxamic Acid Compound and Preparation Method Thereof, and Pharmaceutical Composition Containing This Compound and Use Thereof, 2012. CA2858033C, https://patents.google.com/patent/CA2858033C/en?oq=2858033.
[87] Y. Yao, Z. Tu, C. Liao, Z. Wang, S. Li, H. Yao, Z. Li, S. Jiang, Discovery of novel class i histone deacetylase inhibitors with promising in vitro and in vivo antitumor activities, J. Med. Chem. 58 (2015) 7672–7680, https://doi.org/10.1021/acs.jmedchem.5b01044.
[88] W.W.H. Alan Kozikowski, Jay H. Kalin, Kyle V. Butler, Joel Bergman, Kozikowski, HDAC Inhibitors and Therapeutic Methods Using the Same, US9249087B2, 2016. https://patents.google.com/patent/US9249087B2/en.
[89] P. Angibaud, K. Van Emelen, L. Decrane, S. van Brandt, P. ten Holte, I. Pilatte, B. Roux, V. Poncelet, D. Speybrouck, L. Queguiner, S. Gaurrand, A. Mariën, W. Floren, L. Janssen, M. Verdonck, J. van Dun, J. van Gompel, R. Gilissen, C. Mackie, M. Du Jardin, J. Peeters, M. Noppe, L. Van Hijfte, E. Freyne, M. Page, M. Janicot, J. Arts, Identification of a series of substituted 2-piperazinyl-5-pyrimidylhydroxamic acids as potent histone deacetylase inhibitors, Bioorg. Med. Chem. Lett 20 (2010) 294–298, https://doi.org/10.1016/j.bmcl.2009.10.118.
[90] L. Auzzas, A. Larsson, R. Matera, A. Baraldi, B. Deschênes-Simard, G. Giannini, W. Cabri, G. Battistuzzi, G. Gallo, A. Ciacci, L. Vesci, C. Pisano, S. Hanessian, Non-natural macrocyclic inhibitors of histone deacetylases: design, synthesis, and activity, J. Med. Chem. 53 (2010) 8387–8399, https://doi.org/10.1021/jm101092u.
[91] J.A. Bergman, K. Woan, P. Perez-Villarroel, A. Villagra, E.M. Sotomayor, A. P. Kozikowski, Selective histone deacetylase 6 inhibitors bearing substituted urea linkers inhibit melanoma cell growth, J. Med. Chem. 55 (2012) 9891–9899, https://doi.org/10.1021/jm301098e.
[92] C.B. Botta, W. Cabri, E. Cini, L. De Cesare, C. Fattorusso, G. Giannini, M. Persico, A. Petrella, F. Rondinelli, M. Rodriquez, A. Russo, M. Taddei, Oxime amides as a novel zinc binding group in histone deacetylase inhibitors: synthesis, biological activity, and computational evaluation, J. Med. Chem. 54 (2011) 2165–2182, https://doi.org/10.1021/jm101373a.
[93] X. Cai, H.X. Zhai, J. Wang, J. Forrester, H. Qu, L. Yin, C.J. Lai, R. Bao, C. Qian, Discovery of 7-(4-(3-Ethynylphenylamino)-7-methoxyquinazolin-6-yloxy)-N-hydroxyheptanamide (CUDC-101) as a potent multi-acting HDAC, EGFR, and HER2 inhibitor for the treatment of cancer, J. Med. Chem. 53 (2010), https://doi.org/10.1021/jm901453q, 2000–2009.
[94] Y. Chen, X. Wang, W. Xiang, L. He, M. Tang, F. Wang, T. Wang, Z. Yang, Y. Yi, H. Wang, T. Niu, L. Zheng, L. Lei, X. Li, H. Song, L. Chen, Development of purine-based hydroxamic acid derivatives: potent histone deacetylase inhibitors with marked in vitro and in vivo antitumor activities, J. Med. Chem. 59 (2016) 5488–5504, https://doi.org/10.1021/acs.jmedchem.6b00579.
[95] D. Barnum, J. Greene, A. Smellie, P. Sprague, Identification of common functional configurations among molecules, J. Chem. Inf. Comput. Sci. 36 (1996) 563–571, https://doi.org/10.1021/ci950273r.
[96] G. Luo, F. Lu, L. Qiao, X. Chen, G. Li, Y. Zhang, Discovery of potential inhibitors of aldosterone synthase from Chinese herbs using pharmacophore modeling, molecular docking, and molecular dynamics simulation studies, BioMed Res. Int. 2016 (2016).
[97] R. Muthyala, W.S. Shin, J. Xie, Y.Y. Sham, Discovery of 1-hydroxypyridine-2-thiones as selective histone deacetylase inhibitors and their potential application for treating leukemia, Bioorg. Med. Chem. Lett 25 (2015) 4320–4324, https://doi.org/10.1016/j.bmcl.2015.07.065.
[98] X. Li, Z. Tu, H. Li, C. Liu, Z. Li, Q. Sun, Y. Yao, J. Liu, S. Jiang, Biological evaluation of new largazole analogues: alteration of macrocyclic scaffold with click chemistry, ACS Med. Chem. Lett. 4 (2013) 132–136, https://doi.org/10.1021/ml300371t.
[99] H.Y. Lee, K. Nepali, F.I. Huang, C.Y. Chang, M.J. Lai, Y.H. Li, H.L. Huang, C. R. Yang, J.P. Liou, N-Hydroxycarbonylbenylamino, Quinolines as selective histone deacetylase 6 inhibitors suppress growth of multiple myeloma in vitro and in vivo, J. Med. Chem. 61 (2018) 905–917, https://doi.org/10.1021/acs.jmedchem.7b01404.
[100] M.M. Kemp, Q. Wang, J.H. Fuller, N. West, N.M. Martinez, E.M. Morse, M. Weïwer, S.L. Schreiber, J.E. Bradner, A.N. Koehler, A novel HDAC inhibitor with a hydroxy-pyrimidine scaffold, Bioorg. Med. Chem. Lett 21 (2011) 4164–4169, https://doi.org/10.1016/j.bmcl.2011.05.098.
[101] D.M. Fass, R. Shah, B. Ghosh, K. Hennig, S. Norton, W.N. Zhao, S.A. Reis, P. S. Klein, R. Mazitschek, R.L. Maglathlin, T.A. Lewis, S.J. Haggarty, Short-chain HDAC inhibitors differentially affect vertebrate development and neuronal chromatin, ACS Med. Chem. Lett. 2 (2011) 39–42, https://doi.org/10.1021/ml1001954.
[102] G. Di Pompo, M. Salerno, D. Rotili, S. Valente, C. Zwergel, S. Avnet, G. Lattanzi, N. Baldini, A. Mai, Novel histone deacetylase inhibitors induce growth arrest, apoptosis, and differentiation in sarcoma cancer stem cells, J. Med. Chem. 58 (2015) 4073–4079, https://doi.org/10.1021/acs.jmedchem.5b00126.
[103] Z. Yang, T. Wang, F. Wang, T. Niu, Z. Liu, X. Chen, C. Long, M. Tang, D. Cao, X. Wang, W. Xiang, Y. Yi, L. Ma, J. You, L. Chen, Discovery of selective histone deacetylase 6 inhibitors using the quinazoline as the cap for the treatment of cancer, J. Med. Chem. 59 (2016) 1455–1470, https://doi.org/10.1021/acs.jmedchem.5b01342.
[104] A. Cereto-Massagué, L. Guasch, C. Valls, M. Mulero, G. Pujadas, S. Garcia-Vallvé, DecoyFinder: an easy-to-use python GUI application for building target-specific decoy sets, Bioinformatics 28 (2012) 1661–1662, https://doi.org/10.1093/bioinformatics/bts249.
[105] Y. Kurogi, O. Guner, Pharmacophore modeling and three-dimensional database searching for drug design using Catalyst, Curr. Med. Chem. 8 (2001) 1035–1055, https://doi.org/10.2174/0929867013372481.
[106] T. Sterling, J.J. Irwin, Zinc 15 - ligand discovery for everyone, J. Chem. Inf. Model. 55 (2015) 2324–2337, https://doi.org/10.1021/acs.jcim.5b00559.
[107] A. Alhossary, S.D. Handoko, Y. Mu, C.K. Kwoh, Fast, accurate, and reliable molecular docking with QuickVina 2, Bioinformatics 31 (2015) 2214–2216, https://doi.org/10.1093/bioinformatics/btv082.
[108] O. Trott, A.J. Olson, AutoDock Vina, Improving the speed and accuracy of docking with a new scoring function, efficient optimization, and multithreading, J. Comput. Chem. 31 (2009), https://doi.org/10.1002/jcc.21334. NA-NA.
[109] G.M. Morris, H. Ruth, W. Lindstrom, M.F. Sanner, R.K. Belew, D.S. Goodsell, A. J. Olson, Software news and updates AutoDock4 and AutoDockTools4: automated docking with selective receptor flexibility, J. Comput. Chem. 30 (2009) 2785–2791, https://doi.org/10.1002/jcc.21256.
[110] H. Yang, C. Lou, L. Sun, J. Li, Y. Cai, Z. Wang, W. Li, G. Liu, Y. Tang, AdmetSAR 2.0: web-service for prediction and optimization of chemical ADMET properties, Bioinformatics 35 (2019) 1067–1069, https://doi.org/10.1093/bioinformatics/bty707.
[111] A. Daina, O. Michielin, V. Zoete, SwissADME: a free web tool to evaluate pharmacokinetics, drug-likeness and medicinal chemistry friendliness of small molecules, Sci. Rep. 7 (2017) 1–13, https://doi.org/10.1038/srep42717.
[112] G. Erensoy, K. Ding, C.G. Zhan, A. Elmezayen, K. Yelekçi, M. Duracik, Ö. Bingöl, Özakpinar, İ. Küçükgüzel, Synthesis, in silico studies and cytotoxicity evaluation of novel 1,3,4-oxadiazole derivatives designed as potential mPGES-1 inhibitors, J. Res. Pharm. 24 (2020) 436–451, https://doi.org/10.35333/jrp.2020.187.
[113] J.B. Baell, G.A. Holloway, New substructure filters for removal of pan assay interference compounds (PAINS) from screening libraries and for their exclusion in bioassays, J. Med. Chem. 53 (2010) 2719–2740, https://doi.org/10.1021/jm901137j.
[114] J.C. Phillips, R. Braun, W. Wang, J. Gumbart, E. Tajkhorshid, E. Villa, C. Chipot, R.D. Skeel, L. Kalé, K. Schulten, Scalable molecular dynamics with NAMD, J. Comput. Chem. 26 (2005) 1781–1802, https://doi.org/10.1002/jcc.20289.
[115] B.R. Brooks, C.L. Brooks III, A.D. Mackerell Jr., L. Nilsson, R.J. Petrella, B. Roux, Y. Won, G. Archontis, C. Bartels, S. Boresch, A. Caflisch, L. Caves, Q. Cui, A. R. Dinner, M. Feig, S. Fischer, J. Gao, M. Hodoscek, W. Im, K. Kuczera, T. Lazaridis, J. Ma, V. Ovchinnikov, E. Paci, R.W. Pastor, C.B. Post, J.Z. Pu, M. Schaefer, B. Tidor, R.M. Venable, H.L. Woodcock, X. Wu, W. Yang, D.M. York,

M. Karplus, CHARMM: the biomolecular simulation program, J. Comput. Chem. 30 (2009) 1545–1614, https://doi.org/10.1002/jcc.21287.
[116] J. Lee, X. Cheng, J.M. Swails, M.S. Yeom, P.K. Eastman, J.A. Lemkul, S. Wei, J. Buckner, J.C. Jeong, Y. Qi, S. Jo, V.S. Pande, D.A. Case, C.L. Brooks, A. D. MacKerell, J.B. Klauda, W. Im, CHARMM-GUI input generator for NAMD, GROMACS, AMBER, OpenMM, and CHARMM/OpenMM simulations using the CHARMM36 additive force field, J. Chem. Theor. Comput. 12 (2016) 405–413, https://doi.org/10.1021/acs.jctc.5b00935.
[117] S. Jo, T. Kim, V.G. Iyer, W. Im, CHARMM-GUI: a web-based graphical user interface for CHARMM, J. Comput. Chem. 29 (2008) 1859–1865, https://doi.org/10.1002/jcc.20945.
[118] J. Huang, S. Rauscher, G. Nawrocki, T. Ran, M. Feig, B.L. De Groot, H. Grubmüller, A.D. MacKerell, CHARMM36m: an improved force field for folded and intrinsically disordered proteins, Nat. Methods 14 (2016) 71–73, https://doi.org/10.1038/nmeth.4067.
[119] K. Vanommeslaeghe, A.D. MacKerell, Automation of the CHARMM general force field (CGenFF) I: bond perception and atom typing, J. Chem. Inf. Model. 52 (2012) 3144–3154, https://doi.org/10.1021/ci300363c.
[120] K. Vanommeslaeghe, E.P. Raman, A.D. MacKerell Jr., Automation of the CHARMM General Force Field (CGenFF) II: assignment of bonded parameters and partial atomic charges, J. Chem. Inf. Model. 52 (2012) 3155–3168, https://doi.org/10.1021/ci3003649.
[121] W. Yu, X. He, K. Vanommeslaeghe, A.D. MacKerell Jr., Extension of the CHARMM general force field to sulfonyl-containing compounds and its utility in biomolecular simulations, J. Comput. Chem. 33 (2012) 2451–2468, https://doi.org/10.1002/jcc.23067.
[122] K. Vanommeslaeghe, E. Hatcher, C. Acharya, S. Kundu, S. Zhong, J. Shim, E. Darian, O. Guvench, P. Lopes, I. Vorobyov, A.D. Mackerell, CHARMM general force field: a force field for drug-like molecules compatible with the CHARMM all-atom additive biological force fields, J. Comput. Chem. 31 (2010) 671–690, https://doi.org/10.1002/jcc.21367.
[123] W. Humphrey, A. Dalke, K. Schulten, VMD: Visual molecular dynamics, J. Mol. Graph. 14 (1996) 33–38, https://doi.org/10.1016/0263-7855(96)00018-5.
[124] H. Liu, T. Hou, CaFE: a tool for binding affinity prediction using end-point free energy methods, Bioinformatics 32 (2016) 2216–2218, https://doi.org/10.1093/bioinformatics/btw215.
[125] C. Wang, D. Greene, L. Xiao, R. Qi, R. Luo, Recent developments and applications of the MMPBSA method, Front. Mol. Biosci. 4 (2018) 87. https://www.frontiersin.org/article/10.3389/fmolb.2017.00087.
[126] A.D. Elmezayen, A. Al-Obaidi, A.T. Şahin, K. Yelekçi, Drug repurposing for coronavirus (COVID-19): in silico screening of known drugs against coronavirus 3CL hydrolase and protease enzymes, J. Biomol. Struct. Dyn. (2020) 1–12, https://doi.org/10.1080/07391102.2020.1758791.
[127] A. Al-Obaidi, A.D. Elmezayen, K. Yelekçi, Homology modeling of human GABA-AT and devise some novel and potent inhibitors via computer-aided drug design techniques, J. Biomol. Struct. Dyn. (2020) 1–11, https://doi.org/10.1080/07391102.2020.1774417.
[128] P.A. Kollman, I. Massova, C. Reyes, B. Kuhn, S. Huo, L. Chong, M. Lee, T. Lee, Y. Duan, W. Wang, O. Donini, P. Cieplak, J. Srinivasan, D.A. Case, T.E. Cheatham, Calculating structures and free energies of complex molecules: combining molecular mechanics and continuum models, Acc. Chem. Res. 33 (2000) 889–897, https://doi.org/10.1021/ar000033j.
[129] J. Che, Z. Wang, H. Sheng, F. Huang, X. Dong, Y. Hu, X. Xie, Y. Hu, Ligand-based pharmacophore model for the discovery of novel CXCR2 antagonists as anti-cancer metastatic agents, R. Soc. Open Sci. 5 (2018) 180176, https://doi.org/10.1098/rsos.180176.
[130] S. Haidar, R.W. Hartmann, Computational prediction of new CYP17 inhibitors based on pharmacophore modeling, virtual screening and docking approach, Pharmazie 72 (2017) 529–536, https://doi.org/10.1691/ph.2017.7516.
[131] M. Shahlaei, E. Doosti, Virtual screening based on pharmacophore model followed by docking simulation studies in search of potential inhibitors for p38 map kinase, Biomed. Pharmacother. 80 (2016) 352–372, https://doi.org/10.1016/j.biopha.2016.02.041.
[132] T. Beckers, C. Burkhardt, H. Wieland, P. Gimmnich, T. Ciossek, T. Maier, K. Sanders, Distinct pharmacological properties of second generation HDAC inhibitors with the benzamide or hydroxamate head group, Int. J. Canc. 121 (2007) 1138–1148, https://doi.org/10.1002/ijc.22751.
[133] A.V. Bieliauskas, M.K.H. Pflum, Isoform-selective histone deacetylase inhibitors, Chem. Soc. Rev. 37 (2008) 1402–1413, https://doi.org/10.1039/b703830p.
[134] C.A. Lipinski, Lead- and drug-like compounds: the rule-of-five revolution, Drug Discov. Today Technol. 1 (2004) 337–341, https://doi.org/10.1016/j.ddtec.2004.11.007.
[135] L. Di, E.H. Kerns, Drug-like properties: concepts, structure design and methods from ADME to toxicity optimization. https://doi.org/10.1016/C2013-0-18378-X, 2016.
[136] X.Q. Chen, S.J. Cho, Y. Li, S. Venkatesh, Prediction of aqueous solubility of organic compounds using a quantitative structure-property relationship, J. Pharmacol. Sci. 91 (2002) 1838–1852, https://doi.org/10.1002/jps.10178.
[137] L. Fossati, R. Dechaume, E. Hardillier, D. Chevillon, C. Prevost, S. Bolze, N. Maubon, Use of simulated intestinal fluid for Caco-2 permeability assay of lipophilic drugs, Int. J. Pharm. 360 (2008) 148–155, https://doi.org/10.1016/j.ijpharm.2008.04.034.
[138] B. Press, Optimization of the Caco-2 permeability assay to screen drug compounds for intestinal absorption and efflux, in: K. Turksen (Ed.), Methods Mol. Biol., Humana Press, Totowa, NJ, 2011, pp. 139–154, https://doi.org/10.1007/978-1-61779-191-8_9.
[139] H. Pham-The, T. Garrigues, M. Bermejo, I. González-Álvarez, M.C. Monteagudo, M.Á. Cabrera-Pérez, Provisional classification and in silico study of biopharmaceutical system based on Caco-2 cell permeability and dose number, Mol. Pharm. 10 (2013) 2445–2461, https://doi.org/10.1021/mp4000585.
[140] H. Pham-The, M.Á. Cabrera-Pérez, N.-H. Nam, J.A. Castillo-Garit, B. Rasulev, H. Le-Thi-Thu, G.M. Casañola-Martin, Silico assessment of ADME properties: advances in caco-2 cell monolayer permeability modeling, Curr. Top. Med. Chem. 18 (2018) 2209–2229, https://doi.org/10.2174/1568026619666181130140350.
[141] M.P. Gleeson, D. Gleeson, QM/MM as a tool in fragment based drug discovery. A cross-docking, rescoring study of kinase inhibitors, J. Chem. Inf. Model. 49 (2009) 1437–1448, https://doi.org/10.1021/ci900022h.
[142] D.C. Thompson, C. Humblet, D. Joseph-McCarthy, Investigation of MM-PBSA rescoring of docking poses, J. Chem. Inf. Model. 48 (2008) 1081–1091, https://doi.org/10.1021/ci700470c.
[143] P.D. Lyne, M.L. Lamb, J.C. Saeh, Accurate prediction of the relative potencies of members of a series of kinase inhibitors using molecular docking and MM-GBSA scoring, J. Med. Chem. 49 (2006) 4805–4808, https://doi.org/10.1021/jm060522a.
[144] S. Verma, S. Grover, C. Tyagi, S. Goyal, S. Jamal, A. Singh, A. Grover, Hydrophobic interactions are a key to MDM2 inhibition by polyphenols as revealed by molecular dynamics simulations and MM/PBSA free energy calculations, PloS One 11 (2016), e0149014, https://doi.org/10.1371/journal.pone.0149014.
[145] S.K. Choubey, R. Mariadasse, S. Rajendran, J. Jeyaraman, Identification of novel histone deacetylase 1 inhibitors by combined pharmacophore modeling, 3D-QSAR analysis, in silico screening and Density Functional Theory (DFT) approaches, J. Mol. Struct. 1125 (2016) 391–404, https://doi.org/10.1016/j.molstruc.2016.06.082.
[146] N. Gupta, N. Sitwala, K. Patel, Pharmacophore modelling, validation, 3D virtual screening, docking, design and in silico ADMET simulation study of histone deacetylase class-1 inhibitors, Med. Chem. Res. 23 (2014) 4853–4864, https://doi.org/10.1007/s00044-014-1057-2.
[147] N. Kandakatla, G. Ramakrishnan, Ligand based pharmacophore modeling and virtual screening studies to design novel HDAC2 inhibitors, Adv. Bioinformatics. 2014 (2014) 812148, https://doi.org/10.1155/2014/812148.